Time-dependent mode structure for Lyapunov vectors as a collective movement in quasi-one-dimensional systems

Tooru Taniguchi and Gary P. Morriss
School of Physics, University of New South Wales, Sydney, New South Wales 2052, Australia
(Received 4 June 2004; published 19 January 2005)

The time-dependent mode structure of the Lyapunov vectors associated with the stepwise structure of the Lyapunov spectra and its relation to the momentum autocorrelation function are discussed in quasi-one-dimensional many-hard-disk systems. We obtain the complete mode structures (Lyapunov modes) for all components of the Lyapunov vectors, including the longitudinal and transverse components of both the spatial and momentum parts, and their phase relations. These mode structures are suggested by the form of the Lyapunov vectors for the zero-Lyapunov exponents. The spatial node structures of these modes are explained by the reflection properties of the hard walls used in the models. Our main result is that the largest time-oscillating period of the Lyapunov modes is twice as long as the time-oscillating period of the longitudinal momentum autocorrelation function. This relation is satisfied irrespective of the number of particles and the boundary conditions. A simple explanation for this relation is given based on the form of the time-dependent Lyapunov mode.

DOI: 10.1103/PhysRevE.71.016218 PACS number(s): 05.45.Jn, 05.45.Pq, 02.70.Ns, 05.20.Jj

I. INTRODUCTION

Statistical mechanics based on dynamical instability has drawn considerable attention in recent years. The dynamical instability is described as a rapid separation of two nearby trajectories, the so-called Lyapunov vector, and causes a loss of memory or unpredictability in the dynamical system. The exponential rate of expansion or contraction of the magnitude of the Lyapunov vector is called the Lyapunov exponent, and its positivity, at least for the largest exponent, is a well known indicator of chaos. Many efforts have been devoted to connect the dynamical instability with statistical properties, such as transport coefficients [1,2]. Some works have concentrated on specific effects of the dynamical instability in many-particle systems. Information about the dynamical instability in many-particle systems is given by the complete set of Lyapunov exponents (the Lyapunov spectrum) and their associated Lyapunov vectors. Here, we introduce the Lyapunov spectrum as the ordered set of the Lyapunov exponents $\lambda^{(n)}, n=1,2,\ldots,2dN$, where $\lambda^{(1)} \geqslant \lambda^{(2)} \geqslant \cdots \geqslant \lambda^{(2dN)}$ in d-dimensional systems. The structure of the Lyapunov spectra has been of much interest in many-particle systems and some of the results obtained have been the conjugate pairing rule for the Lyapunov spectra of thermostated systems [3–6], the localized behavior of Lyapunov vectors [7–11], and the thermodynamic limit of Lyapunov spectra [12–15].

The stepwise structure of the Lyapunov spectra is one of such chaotic properties of many-particle systems, which was found recently [16]. This stepwise structure appears in the Lyapunov exponents with smallest absolute value, and the dynamical structure of these Lyapunov exponents should reflect slow and global behavior of the macroscopic system. Therefore, clarification of the stepwise structure of Lyapunov spectra (Lyapunov steps) is expected to make a bridge between the macroscopic statistical theory and microscopic chaotic dynamics. The Lyapunov steps accompany wavelike structures in the associated Lyapunov vectors (the Lyapunov modes), which offer a useful tool to understand the origin of the stepwise structure of the Lyapunov spectrum [17–20]. Originally, these structures were observed in many-hard-disk systems, but very recently numerical evidence for the Lyapunov modes was reported for many-particle systems with soft-core particle interactions [21,22]. Some theoretical arguments have been proposed to explain this phenomenon, for example, using random matrix theory [23,24], kinetic theory [25–27], and periodic orbit theory [15], etc.

The key to understanding the Lyapunov steps and modes is in the zero-Lyapunov exponents and their associated Lyapunov vectors. Using the notation $\delta\mathbf{\Gamma}^{(n)}=(\delta\mathbf{q}^{(n)},\delta\mathbf{p}^{(n)})=(\delta\mathbf{q}_x^{(n)},\delta\mathbf{q}_y^{(n)},\delta\mathbf{p}_x^{(n)},\delta\mathbf{p}_y^{(n)})$ for the Lyapunov vector corresponding to Lyapunov exponent $\lambda^{(n)}$, the Lyapunov vectors corresponding to the six zero-Lyapunov exponents of a two-dimensional system of N hard particles in periodic boundary conditions can be written as linear combinations of the six basis vectors $N^{-1/2}(\mathbf{1},\mathbf{0},\mathbf{0},\mathbf{0})$, $N^{-1/2}(\mathbf{0},\mathbf{1},\mathbf{0},\mathbf{0})$, $N^{-1/2}(\mathbf{0},\mathbf{0},\mathbf{1},\mathbf{0})$, $N^{-1/2}(\mathbf{0},\mathbf{0},\mathbf{0},\mathbf{1})$, $|\mathbf{p}|^{-1}(\mathbf{p}_x,\mathbf{p}_y,\mathbf{0},\mathbf{0})$, and $|\mathbf{p}|^{-1}(\mathbf{0},\mathbf{0},\mathbf{p}_x,\mathbf{p}_y)$. Here $\mathbf{0}$ is an N-dimensional null vector, $\mathbf{1}$ is an N-dimensional vector with all components equal to 1, and $\mathbf{p}\equiv(\mathbf{p}_x,\mathbf{p}_y)$ is the momentum vector with its x component $\mathbf{p}_x$ and y component $\mathbf{p}_y$. Here, the first (second) basis vector is associated with the translational invariance in the x direction (y direction), the third (fourth) basis vector with the conservation of the x component (y component) of the total momentum, the fifth basis vector with the time-translational invariance (deterministic nature of the orbit), and the last basis vector with the energy conservation [1]. This means that the six sets of the Lyapunov vector components $\{\delta x_j^{(n)}\}_j$, $\{\delta y_j^{(n)}\}_j$, $\{\delta p_{xj}^{(n)}\}_j$, $\{\delta p_{yj}^{(n)}\}_j$, $\{\delta x_j^{(n)}/p_{xj}, \delta y_j^{(n)}/p_{yj}\}_j$, and $\{\delta p_{xj}^{(n)}/p_{xj}, \delta p_{yj}^{(n)}/p_{yj}\}_j$ (where $\delta x_j^{(n)}$ is the jth component of $\delta\mathbf{q}_x^{(n)}$, etc.) can have equal components independent of the particle index j for the zero-Lyapunov exponent modes.

We regard the degeneracy of the zero-Lyapunov exponents and the structure of the corresponding Lyapunov vec-

tors as the zeroth Lyapunov step and mode. This scenario was proposed first in Ref. [18], and was also discussed very recently in Ref. [20]. First of all, the Lyapunov steps for the rectangular two-dimensional system with periodic boundary conditions consist of two-point steps and four-point steps [17,18], namely, the number of Lyapunov exponents for one set of Lyapunov steps is six, which is equal to the number of the zero-Lyapunov exponents. It is also known that the stepwise structure of Lyapunov spectra is changed by violating the spatial translational invariance and the total momentum conservation, which also change the number of zero-Lyapunov exponents [18]. As a second point, some mode structures were observed in some of the above Lyapunov vector components, which should be constant in zero-Lyapunov exponents. For example, a mode structure in the Lyapunov vector component $\delta y_j^{(n)}$ (the transverse spatial translational invariance Lyapunov mode) is well known [17]. This mode is stationary in time, and appears in one of the two types of the Lyapunov steps. Reference [18] showed another mode structure in $\delta y_j^{(n)}/p_{yj}$ (the transverse time translational Lyapunov mode). This mode depends on time, and appears in other types of the Lyapunov steps. These Lyapunov modes are enough to categorize all the Lyapunov steps. References [17,19] also claim a moving mode structure in $\delta x_j^{(n)}$.

However, there is not enough evidence yet to confirm the above scenario for the Lyapunov steps and modes. For example, the mode structure in the momentum part of Lyapunov vectors has not been reported explicitly. Besides, the phase relations of different modes, for example the modes in $\delta y_j^{(n)}/p_{yj}$ and $\delta x_j^{(n)}$, have not been discussed. Another important problem is the time scale specified by a time-dependent Lyapunov mode, like the time oscillation for the mode in $\delta y_j^{(n)}/p_{yj}$. The time-oscillating period is usually much longer than the mean free time of the system, and it should correspond to a collective movement, but quantitative evidence for it has not been shown clearly.

As an indicator for collective movements of many-particle systems, we can use the momentum autocorrelation functions, where collective movement may appear as a time-oscillation behavior [28], as observed in many macroscopic models [29–33]. The autocorrelation functions are accessible experimentally using neutron and light scattering techniques [33–36]. An essential aspect of autocorrelation functions is their role as response functions for the system. For example, linear-response theory connects the time integral of the autocorrelation function with a transport coefficient [37]. However, it should be emphasized that the autocorrelation functions themselves provide much more detailed information about the system. Linear-response theory requires the time-integral and the thermodynamic limit of the autocorrelation function to calculate transport coefficients, and in this process information about short time scales and finite-size effects is lost. For instance, the time oscillation of the autocorrelation functions is one of the finite-size effects, which linear-response theory does not treat. Information on short time scales and finite-size effects in the autocorrelation functions also plays an important role in the generalized hydrodynamics [38] and generalized Fokker-Planck equation [39].

The purposes of this paper are twofold. First we calculate all components of the Lyapunov vectors associated with the stepwise structure of the Lyapunov spectrum. They include the longitudinal and transverse components of both the spatial and momentum parts of the Lyapunov vectors. We demonstrate the wavelike structures in the components of the Lyapunov vectors, and specify their phase relations. These results support the above explanation for the origin of the Lyapunov steps and modes based on the zero-Lyapunov exponents and the associated Lyapunov vectors. Spatial node structures of these Lyapunov modes are explained in terms of boundary conditions. It is emphasized that some of the Lyapunov modes show time-oscillating behaviors, and particle number dependence in their time-oscillating periods. The second purpose of this paper is to discuss the connection between the time oscillation of the Lyapunov modes and the momentum autocorrelation functions. It is shown that the largest time-oscillating period of the Lyapunov modes is twice as long as that for a momentum autocorrelation function. This gives some evidence to connect the Lyapunov modes, a tangent space property, to the autocorrelation function, which is a phase-space property that is accessible experimentally.

As a simple many-particle chaotic model, in this paper we use a quasi-one-dimensional many-hard-disk system [11,18]. This model allows fast numerical calculation of the Lyapunov exponents and vectors, and shows clear Lyapunov steps and modes. These features of this model are advantageous to the aim of this paper, because in general the numerical calculation of the Lyapunov spectrum and vectors is very time-consuming, and it is often difficult to get clear Lyapunov mode structures, particularly for time-dependent Lyapunov modes. Besides, if the above picture of the Lyapunov steps and modes based on universal properties such as the translational invariances and the conservation laws can be justified, then such a simple model should be sufficient to convince us of their origin. This system also exhibits a clear oscillatory behavior in the longitudinal momentum autocorrelation function. Another useful technique to get clear Lyapunov steps and modes is to use hard-wall boundary conditions. Although hard-wall boundary conditions destroy the spatial translational invariance and the total momentum conservation, and lead to different structure in the Lyapunov spectrum compared to periodic boundary conditions, it has been shown that there is a simple relation between the observed Lyapunov steps and modes and different boundary conditions [18]. Specifically, we use a quasi-one-dimensional system with hard-wall boundary conditions in the longitudinal direction and periodic boundary conditions in the transverse direction. Usually, the hard-wall boundary conditions make numerical calculation slower compared to periodic boundary conditions, but in our system only the two particles at each end of the system collide with the hard walls, so the effect is small.

The outline of this paper is as follows. In Sec. II, the quasi-one-dimensional system is introduced. In Sec. III, we discuss the Lyapunov steps and modes. In Sec. IV, the momentum autocorrelation functions and their relation with the Lyapunov modes are discussed. Finally, we give some conclusion and remarks in Sec. V.

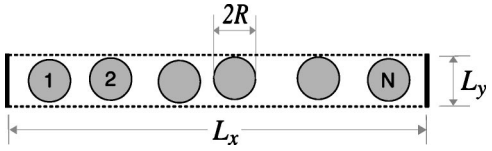

FIG. 1. A schematic illustration of the quasi-one-dimensional system. The system shape is so narrow that particles always remain in the same order. Here, $L_x(L_y)$ is the length (width) of the system in the longitudinal (transverse) direction, and R is the radius of a particle. The solid lines represent hard-wall boundary conditions (H), and the dashed lines represent periodic boundary conditions (P), representing the boundary condition (H,P). The particles are numbered $1,2,\ldots,N$ from the left to the right.

II. QUASI-ONE-DIMENSIONAL SYSTEM

The model considered in this paper is a quasi-one-dimensional many-hard-disk system. It is a two-dimensional rectangular system consisting of many hard disks with the width of the system so narrow that the disk positions are not exchanged, thus the disks can be numbered from left to right. We assume that the mass m and the radius R of each disk is the same. In this case, the quasi-one-dimensional system has a width L_y that satisfies the condition $2R<L_y<4R$. Figure 1 gives a schematic illustration of the quasi-one-dimensional system with the particles numbered $1,2,\ldots,N$ (N is the particle number) from the left to right.

Originally, the quasi-one-dimensional many-hard-disk system was introduced as a system to easily and clearly observe the stepwise structure of the Lyapunov spectrum and the corresponding wavelike structure of Lyapunov vectors [18]. Numerical observation of the Lyapunov steps and modes is very time-consuming, and even at present the Lyapunov spectrum is limited to about 1000 particles [17]. Therefore, it is valuable to explore fast and efficient ways to calculate them numerically. It is well known that the rectangular system has a wider stepwise region than a square system with the same area and number of particles. This quasi-one-dimensional system is the most rectangular two-dimensional system possible. Reference [18] demonstrated that in the quasi-one-dimensional system we can clearly observe the structure of the Lyapunov modes. It is known that there are two kinds of Lyapunov modes: stationary modes and time-dependent modes. The stationary Lyapunov modes are most easily observed because of their stable structure, but generally the observation of the time-dependent Lyapunov modes is much harder because of large fluctuations in their structure and their intrinsic time dependence. The quasi-one-dimensional system is the first system in which time-oscillating Lyapunov modes were demonstrated [18].

Another advantage of the quasi-one-dimensional system is that the particle interactions in this system are restricted to nearest-neighbor particles only, so we need much less effort to find colliding particle pairs numerically compared with the fully two-dimensional system in which each particle can collide with any other particle. This leads to faster numerical calculation of the system dynamics. Besides, in this system, particle movement in the narrow direction is suppressed, compared to the longitudinal direction, and roughly speaking the particle sequence corresponds to the particle position. This leads to a much simpler representation of Lyapunov modes, which must be investigated as functions of spatial coordinates and time. One may also notice that in the quasi-one-dimensional system, the system size is proportional to the particle number N, while for the square system it is proportional to $\sqrt{N}$. This implies that in the quasi-one-dimensional system, many-particle effects are more evident than for the fully two-dimensional systems with the same number of particles.

Another important point in the quasi-one-dimensional system is the effect of boundary conditions. Different from the square system, in which the boundary length is proportional to the square root of the system size, in the quasi-one-dimensional system the boundary length is proportional to the system size itself, therefore we cannot neglect its effect even in the thermodynamic limit. Actually, Ref. [18] showed that the Lyapunov steps and modes depend strongly on boundary conditions. Boundary conditions change not only the structure of Lyapunov steps and modes, but also the clearness of Lyapunov mode structure. For example, a system with purely hard-wall boundary conditions has no stationary Lyapunov mode and its corresponding Lyapunov steps and shows much clearer time-oscillating Lyapunov modes, compared to a system with periodic boundary conditions. Roughly speaking, hard-wall boundary conditions pin the positions of the nodes and thus lead to clearer Lyapunov modes. On the other hand, the numerical calculation with the hard-wall boundary conditions is more time-consuming. This disadvantage is significant in the quasi-one-dimensional system with purely hard-wall boundary conditions. As another disadvantage of the system with purely hard-wall boundary conditions, we cannot investigate the stationary Lyapunov mode due to spatial translational invariance. As an optimal system, in this paper we mostly consider a quasi-one-dimensional system with hard-wall boundary conditions in the longitudinal direction and periodic boundary conditions in the transverse direction. We use the notation (H,P) for this boundary condition throughout this paper. In Fig. 1, we represent the boundary condition (H,P) as different types of lines on the boundaries: the bold solid lines signify hard-wall boundary conditions and the broken lines signify periodic boundary conditions.

Although the quasi-one-dimensional many-hard-disk system with the boundary condition (H,P) may be artificially introduced to investigate Lyapunov steps and modes in a fast and effective way, it is essential to note that the results from this system can be used to predict Lyapunov steps and modes in more general systems, such as a fully two-dimensional system with purely periodic boundary conditions. Details of the relation of the Lyapunov steps and modes in quasi-one-dimensional systems with different boundary conditions were given in Ref. [18]. For example, the step widths of the Lyapunov spectrum (the spatial and time periods of the corresponding Lyapunov modes) in the system with the boundary condition (H,P) are halves (twice) the ones in the system with the purely periodic boundary conditions (P,P). It is also known that the structure of Lyapunov steps for the quasi-one-dimensional system is the same as the fully two-dimensional rectangular system.

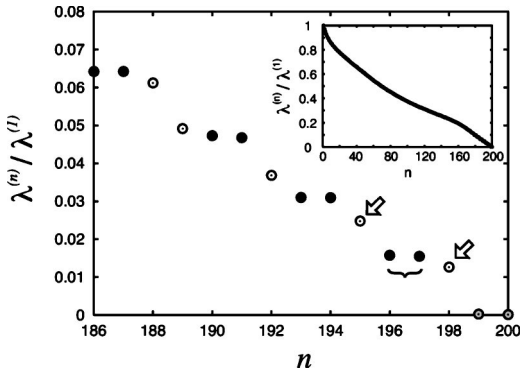

FIG. 2. Stepwise structure of the Lyapunov spectrum normalized by the largest Lyapunov exponent for the quasi-one-dimensional system with $N=100$ and (H,P) boundary conditions. The white-filled (black-filled) circles correspond to the stational (time-oscillating) Lyapunov modes. Inset: The full spectrum of the positive branch of the normalized Lyapunov spectrum. Note that the step structure dissolves at about exponent number 160 so this effect is only seen in the slowest modes.

As we discussed above, the main reason to use the quasi-one-dimensional system with the boundary condition (H,P) is to get clear Lyapunov steps and modes in a fast numerical calculation. On the other hand, these advantages may not assist the calculation of the momentum autocorrelation function. In the quasi-one-dimensional system, collisions of a particle are restricted to its two nearest-neighbor particles only, so it may be supposed that specific types of collisions like the "backscattering effect" play an important role. The backscattering effect, which comes from a reversal of the velocity of a particle by a collision with the nearest-neighbor particle, can lead to a negative region of the momentum autocorrelation function. One may also suppose that in the quasi-one-dimensional system, a collective motion may be enhanced, because the movement of particles in the narrow direction is very restricted. This may lead to a clear time oscillation of the momentum autocorrelation function, as will be observed in Sec. IV. It may also be noted that boundary condition effects on the momentum autocorrelation function are not well known. Because we need to know about them to be able to guess the relation between the autocorrelation functions and Lyapunov modes in different boundary conditions, we will discuss the boundary condition effects on the momentum autocorrelation function briefly in Sec. IV C.

In this paper, we use units where the mass m and the particle radius R are 1, and the total energy E is N (except in Sec. III D). For the numerical calculations, the system lengths are chosen as $L_x=1.5NL_y+2R$ and $L_y=2R(1+10^{-6})$ for the quasi-one-dimensional system with the boundary condition (H,P). The density is $\rho=N\pi R^2/\bar{V}$, where $\bar{V}$ is the volume accessible to the center of the particle.

III. LYAPUNOV STEPS AND MODES

In this section, we discuss the Lyapunov steps and modes in the quasi-one-dimensional system with boundary condition (H,P). Part of these results have already been presented

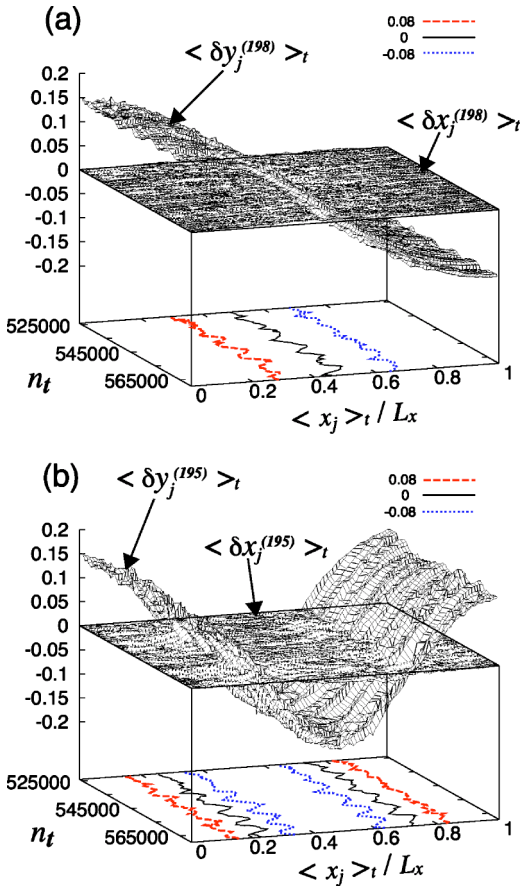

FIG. 3. (Color online) Local time averages of $\langle \delta x_j \rangle_t$ and $\langle \delta y_j \rangle_t$ for the first two-point step (exponent 198) in (a), and for the second two-point step (exponent 195) in (b). These are shown as functions of the collision number n_t and the normalized local time average $\langle x_j \rangle_t / L_x$ of the x component of the jth particles position (with the system length L_x). The corresponding Lyapunov exponents $\lambda^{(198)}$ and $\lambda^{(195)}$ are indicated by arrows in Fig. 2. On the base of each graph are the contour plots of the transverse Lyapunov modes at the levels −0.08 (dotted lines), 0 (solid lines), and +0.08 (broken lines).

in Ref. [18], and here we complete this presentation. Some of the discussions omitted in Ref. [18] were the relation between the time-oscillating Lyapunov mode proportional to the momentum and the longitudinal Lyapunov modes, the Lyapunov modes for the momentum parts of Lyapunov vectors, and the particle number dependence of the time-oscillating period of the Lyapunov modes.

For a numerical calculation of the Lyapunov spectrum and the Lyapunov vectors, we used the numerical algorithm developed by Benettin *et al.* [40] and Shimada *et al.* [41] (also see Refs. [42,43]). This algorithm is characterized by regular reorthogonalizations and renormalization of the set of Lyapunov vectors, which is done after each particle collision. Usually the Lyapunov steps and modes appear after a long trajectory calculation, and we typically calculated trajectories of more than 5×10^5 particle collisions to get the Lyapunov spectra and vectors. Typically, the zero-Lyapunov exponents converge first, followed by the next smallest exponents, with the higher steps being last to converge.

The main purpose of this section is to investigate the time-oscillating structures in the longitudinal momentum

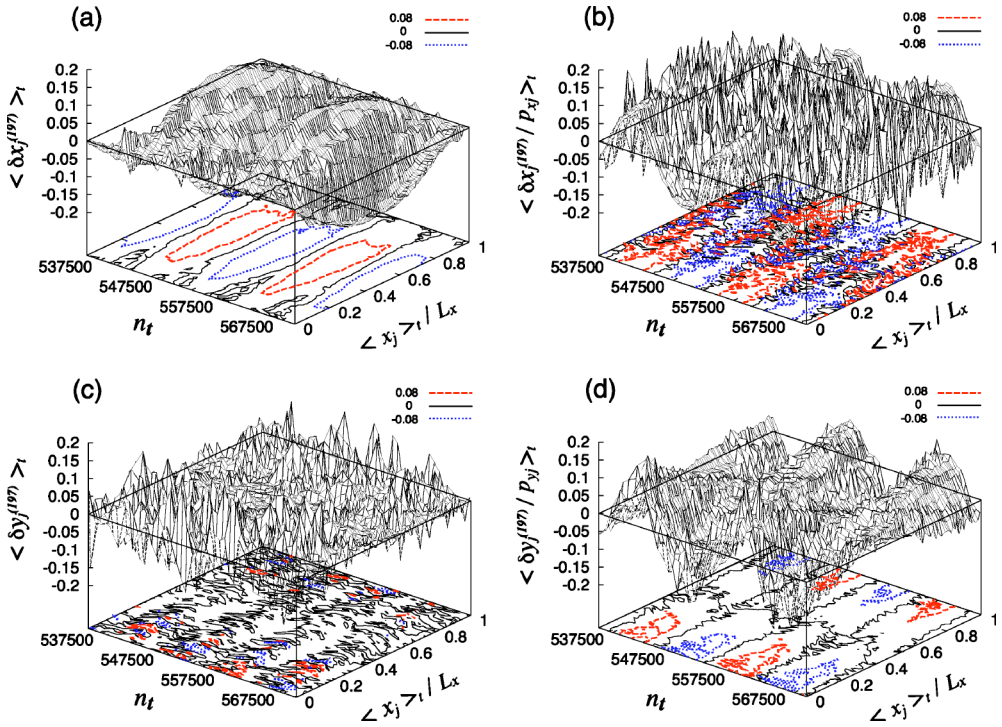

FIG. 4. (Color online) Local time averages of $\langle \delta x_j \rangle_t$, $\langle \delta x_j / p_{xj} \rangle_t$, $\langle \delta y_j \rangle_t$, and $\langle \delta y_j / p_{yj} \rangle_t$ for the Lyapunov modes corresponding to the first exponent of the first two-point step ($\lambda^{(197)}$), as functions of the collision number n_t and the normalized local time average $\langle x_j \rangle_t / L_x$ of the x component of the position of the jth particle. The base of each graph is a contour plot of the three-dimensional graph at the levels −0.08 (dotted lines), 0 (solid lines), and +0.08 (broken lines).

proportional Lyapunov modes. We present results for 100-particle systems, and in such small systems the structure of the Lyapunov modes has large fluctuations in space and time which can obscure the appearance of clear mode structures. Another problem appears for the Lyapunov modes that are proportional to the momentum. We investigate these modes by calculating such quantities as $\delta x_j^{(n)}/p_{xj}$, which should show a time-oscillating wavelike structure, if the Lyapunov vector components have modes proportional to momentum. However, fluctuations of this quantity may be enhanced in cases when the momentum component is close to zero. To overcome these technical problems, and to visualize this structure as clearly as possible, we take a local time average of the Lyapunov modes. More concretely, for the Lyapunov vector components $\delta x_j^{(n)}$ and $\delta y_j^{(n)}$, we take their arithmetic average over $8N$ collisions using data just after collisions, and plot them as functions of the same local time average of x_j and the first collision number of time interval. For modes in the quantities $\delta x_j^{(n)}/p_{xj}$, $\delta y_j^{(n)}/p_{yj}$, $\delta p_{yj}^{(n)}/p_{xj}$, and $\delta p_{yj}^{(n)}/p_{yj}$, we take the same local time average, except that if the absolute value $|p_{xj}|$ ($|p_{yj}|$) is less than 10% of the averaged momentum amplitude $\sqrt{2mE/N}$, then we exclude the data at that time from the local time average. We use the notation $\langle \cdots \rangle_t$ for such a local time average.

A. Lyapunov steps

Figure 2 is the stepwise structure of the Lyapunov spectrum normalized by the largest Lyapunov exponent for the quasi-one-dimensional many-hard-disk system of 100 particles with (H,P) boundary condition. The entire positive branch of the Lyapunov spectrum is shown in the inset to this figure. In a Hamiltonian system, the negative branch of the Lyapunov spectrum takes the same absolute value as the positive branch of the Lyapunov spectrum from the conjugate pairing rule: $\lambda^{(4N-n+1)}=-\lambda^{(n)}$, $n=1,2,\ldots,2N$ [44], so they are omitted in Fig. 2.

This system has four zero-Lyapunov exponents, which come from the conservation of the y component of the total momentum and the center of mass, energy conservation, and the deterministic nature of the orbit. Note that the x component of the total momentum and the center of mass are not conserved, because of the hard-wall boundary condition in the x direction. Exponents number 199, 200, 201, and 202 are zero in Fig. 2.

The stepwise structure of the Lyapunov spectrum in this system consists of one- and two-point steps. These two kinds of Lyapunov steps accompany different mode structures in the Lyapunov vectors: one is the stationary modes, as discussed in Sec. III B, and the other is time-oscillating modes, as discussed in Sec. III C. Here we count the sequence of Lyapunov steps from the zero-Lyapunov exponents $\lambda^{(200)}$ and $\lambda^{(199)}$, so $\lambda^{(198)}$ is the first one-point step, $\lambda^{(197)}$ and $\lambda^{(196)}$ are the first two-point step, $\lambda^{(195)}$ is the second one-point step, and $\lambda^{(194)}$ and $\lambda^{(193)}$ are the second two-point step, see Fig. 2.

B. Stationary Lyapunov modes

First we discuss the Lyapunov mode corresponding to the first and second one-point steps in Fig. 2. Figure 3 shows the

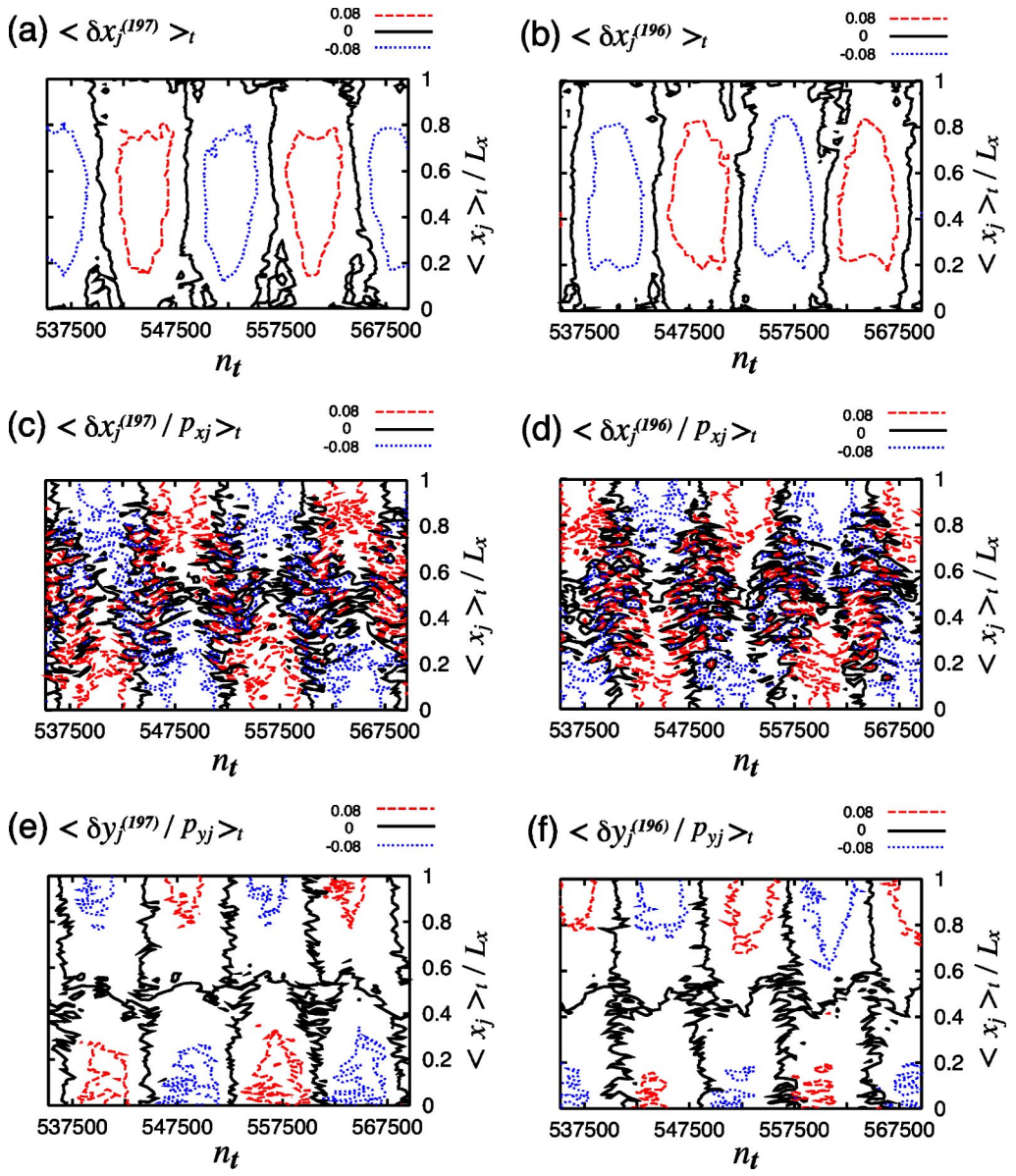

FIG. 5. (Color online) Contour plots of the local time averages of $\langle \delta x_j \rangle_t$, $\langle \delta x_j / p_{xj} \rangle_t$, $\langle \delta y_j / p_{yj} \rangle_t$, for the first two-point steps [$\lambda^{(197)}$ (a,c,e) and $\lambda^{(196)}$ (b,d,f)], as functions of the collision number n_t and the normalized local time average $\langle x_j \rangle_t / L_x$ of the position of the jth particle in the same collision number interval [535200, 569600]. The dotted lines, the solid lines, and the broken lines are contour lines at the levels −0.08, 0, and +0.08, respectively.

graph of the Lyapunov vector components corresponding to the first and second one-point step as a function of the collision number n_t and the normalized local time average $\langle x_j \rangle_t / L_x$ of the x component of the particle position. Here, Fig. 3(a) is for the local time averages of $\langle \delta x_j^{(198)} \rangle_t$ and $\langle \delta y_j^{(198)} \rangle_t$ for the first one-point step $\lambda^{(198)}$, and Fig. 3(b) is a similar graph for the second one-point step $\lambda^{(195)}$. These one-point steps are indicated by arrows in Fig. 2. Both graphs have the same collision number interval [524000,569600]. On the base of each of Figs. 3(a) and 3(b), we give contour plots of the transversal modes $\langle \delta y_j^{(198)} \rangle_t$ and $\langle \delta y_j^{(195)} \rangle_t$, respectively, in which the dotted lines, the solid lines, and the broken lines correspond to the levels −0.08, 0, and +0.08, respectively.

In Fig. 3, we recognize spatial wavelike structures in the transverse components of $\langle \delta y_j^{(n)} \rangle_t$ for $n=198$ and 195, which are stationary in time (at least in a time interval of more than 45×10^3 collisions as shown in this figure). These wavelike structures are very nicely fitted by sinusoidal functions [18]. Note that the numerical algorithm ensures that the Lyapunov vectors are normalized, so that the amplitudes of any component of the Lyapunov vector must be less than 1. It should be emphasized that antinodes in the modes appear at the end of the system in the x direction. By comparison, the amplitudes of the longitudinal components of $\langle \delta x_j^{(n)} \rangle_t$ for $n=198$ and 195 are extremely small. These observations suggest that the Lyapunov mode corresponding to the kth one-point Lyapunov step is approximately represented by

$$\begin{pmatrix} \delta x_j^{(\mu(k))} \\ \delta y_j^{(\mu(k))} \end{pmatrix} = \alpha_k \begin{pmatrix} 0 \\ 1 \end{pmatrix} \cos\left(\frac{\pi k}{L_x} x_j \right), \tag{1}$$

where α_k is a constant and $\mu(k)$ is the Lyapunov index corresponding to the kth one-point step of the Lyapunov spectrum. Here we take the origin of the x component of the spatial coordinate to be $x_j = 0$, so that an ambiguity in spatial phase can be removed in Eq. (1).

C. Time-oscillating Lyapunov modes

Now we discuss the remaining Lyapunov modes, which correspond to the two-point steps of the Lyapunov spectrum. Figure 4 shows the graphs of the local time averages of $\langle \delta x_j^{(197)} \rangle_t$, $\langle \delta x_j^{(197)} / p_{xj} \rangle_t$, $\langle \delta y_j^{(197)} \rangle_t$, and $\langle \delta y_j^{(197)} / p_{yj} \rangle_t$ as functions of the collision number n_t and normalized local time-averaged position $\langle x_j \rangle_t / L_x$ of the jth particle. The number of particles is $N = 100$, and the four graphs are for the same collision number interval $n_t \in [535200, 569600]$. These correspond to the first exponent of the first two-point step, exponent 197.

We can easily recognize spatial wavelike structures with time oscillations in Figs. 4(a) and 4(d). In Fig. 4(a), the longitudinal Lyapunov vector component $\langle \delta x_j^{(197)} \rangle_t$ has nodes at the ends of the quasi-one-dimensional system, and the wavelength is given by $2L_x$. On the other hand, in Fig. 4(d), the transverse Lyapunov vector component $\langle \delta y_j^{(197)} / p_{yj} \rangle_t$ has antinodes at the end of the system and has a node at the middle, although its wavelength is given by $2L_x$ as for the longitudinal mode of Fig. 4(a).

There is also a time-oscillating wavelike structure in the longitudinal Lyapunov vector component $\langle \delta x_j^{(197)} / p_{xj} \rangle_t$, as shown in Fig. 4(b). This structure is different from the one shown in Fig. 4(a) associated with the same longitudinal Lyapunov vector component $\delta x_j^{(197)}$. It has antinodes at the ends of the system, and has a node in the middle. Its wavelength is $2L_x$. These characteristics suggest that although there are large fluctuations in the middle of the system, the time-oscillating wavelike structure in Fig. 4(b) is the same as that in Fig. 4(d). In Fig. 4(c), it is rather difficult to recognize any structure. Roughly speaking, it is just random fluctuations, but the amplitude of such fluctuations in the middle of the system is small compared to the region at the end of the system. However, such small-amplitude fluctuations are required for consistency with Fig. 4(d), namely, the fact that in this region the value of $\delta y_j^{(197)} / p_{yj}$ is small, so the value of $\delta y_j^{(197)}$ itself should be small with an almost position-independent momentum p_{yj}.

Next we discuss the phase relations for the Lyapunov modes of the first two-point steps, corresponding to exponents $\lambda^{(196)}$ and $\lambda^{(197)}$ (the black-filled circles with brace underneath in Fig. 2). Figure 5 shows the contour plots of the local time averages of $\langle \delta x_j \rangle_t$, $\langle \delta x_j / p_{xj} \rangle_t$, $\langle \delta y_j / p_{yj} \rangle_t$, and for $\lambda^{(196)}$ and $\lambda^{(197)}$ as functions of the collision number n_t and the normalized local time average $\langle x_j \rangle_t / L_x$ of the position of the jth particle for a 100-particle system. The six graphs in Fig. 5 have the same collision number interval [535200, 569600], and Figs. 5(a), 5(c), and 5(e) correspond to Figs. 4(a), 4(b), and 4(d)

Figure 5 shows that the two Lyapunov exponents for the same two-point step have the same structure of Lyapunov modes, but they are orthogonal in time, namely, nodal lines of the Lyapunov modes corresponding to the exponent $\lambda^{(197)}$ correspond to antinodal lines of exponent $\lambda^{(196)}$. We also notice that the nodal lines of the Lyapunov modes in $\langle \delta x_j^{(n)} / p_{xj} \rangle_t$ and $\langle \delta y_j^{(n)} / p_{yj} \rangle_t$ coincide with each other in space and time ($n = 197, 196$), on the other hand the Lyapunov modes in $\langle \delta x_j^{(n)} \rangle_t$ and $\langle \delta x_j^{(n)} / p_{xj} \rangle_t$ are orthogonal in space and time at the same Lyapunov index.

The above discussions based on Figs. 4 and 5 (and similar observations of Lyapunov modes in the other two-point steps of the Lyapunov spectrum) lead to the conjecture that the spatial part of Lyapunov vector components $\delta x_j^{(\nu(k))}$ and $\delta y_j^{(\nu(k)-1)}$ corresponding to the Lyapunov exponents of the kth two-point step are approximately expressed as

$$\begin{pmatrix} \delta x_j^{(\nu(k))} \\ \delta y_j^{(\nu(k))} \end{pmatrix} = \alpha_k' \begin{pmatrix} p_{xj} \\ p_{yj} \end{pmatrix} \cos\left(\frac{\pi k}{L_x} x_j \right) \cos\left(\frac{2\pi k}{T_{\mathrm{Lya}}} n_t + \beta_k' \right) + \tilde{\alpha}_k' \begin{pmatrix} 1 \\ 0 \end{pmatrix} \sin\left(\frac{\pi k}{L_x} x_j \right) \sin\left(\frac{2\pi k}{T_{\mathrm{Lya}}} n_t + \beta_k' \right), \tag{2}$$

$$\begin{pmatrix} \delta x_j^{(\nu(k)-1)} \\ \delta y_j^{(\nu(k)-1)} \end{pmatrix} = \alpha_k'' \begin{pmatrix} p_{xj} \\ p_{yj} \end{pmatrix} \cos\left(\frac{\pi k}{L_x} x_j \right) \sin\left(\frac{2\pi k}{T_{\mathrm{Lya}}} n_t + \beta_k' \right) + \tilde{\alpha}_k'' \begin{pmatrix} 1 \\ 0 \end{pmatrix} \sin\left(\frac{\pi k}{L_x} x_j \right) \cos\left(\frac{2\pi k}{T_{\mathrm{Lya}}} n_t + \beta_k' \right), \tag{3}$$

with α_k', α_k'', $\tilde{\alpha}_k'$, $\tilde{\alpha}_k''$, and β_k' constants. It should be noted that large fluctuations in the Lyapunov mode represented in the middle of Figs. 4(b), 5(c), and 5(d), can come from the x components of the second terms on the right-hand sides of the vectors (2) and (3). On the other hand, the effect of the x components of the first terms on the right-hand side of the vectors (2) and (3) does not appear explicitly in Figs. 4(a), 5(a), and 5(b), because the factor p_{xj} in these terms distributes their contributions randomly and these terms disappear after taking local time averages.

D. Energy dependence of Lyapunov mode amplitudes

In expressions (2) and (3) for the time-oscillating Lyapunov modes, the quantities α_k', α_k'', $\tilde{\alpha}_k'$, and $\tilde{\alpha}_k''$ are intro-

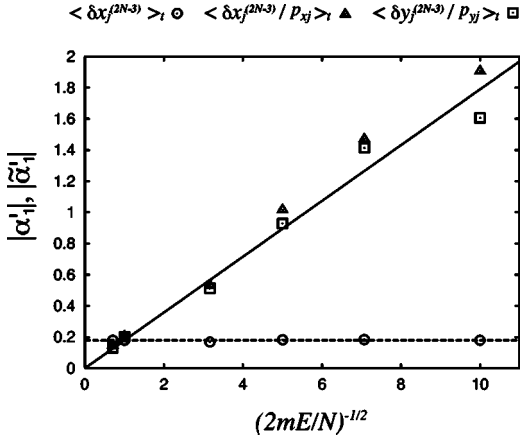

FIG. 6. Amplitudes $|\alpha_1'|$ and $|\tilde{\alpha}_1'|$ of Lyapunov modes $\langle \delta x_j^{(2N-3)} \rangle_t$ (circles), $\langle \delta x_j^{(2N-3)}/p_{xj} \rangle_t$ (triangles), and $\langle \delta y_j^{(2N-3)}/p_{yj} \rangle_t$ (squares) as functions of $1/\sqrt{2mE/N}$ in the quasi-one-dimensional system of 50 hard disks with (H,P) boundary condition. The broken line is a fit of the amplitude $|\tilde{\alpha}_1'|$ to a constant function $|\tilde{\alpha}_1'| = \xi$ with a fitting parameter ξ, and the solid line is given by a linear function $\xi/\sqrt{2mE/N}$.

duced simply as coefficients of the linear combination of the longitudinal spatial translational invariance Lyapunov mode and the time translational invariance Lyapunov mode. However, it is important to note that these coefficients are related to each other through the normalization of the Lyapunov mode.

As the Lyapunov mode vector is normalizable, this leads to the approximate relations

$$|\alpha_k'| \approx \frac{|\tilde{\alpha}_k'|}{\sqrt{2mE/N}}, \tag{4}$$

$$|\alpha_k'| \approx |\alpha_k''|, \tag{5}$$

$$|\tilde{\alpha}_k'| \approx |\tilde{\alpha}_k''|, \tag{6}$$

with the mass m (=1), the total energy E, and the number of particles N.

In Fig. 6, we show the amplitudes $|\alpha_1'|$ and $|\tilde{\alpha}_1'|$, which are obtained by fitting the Lyapunov modes $\langle \delta x_j^{(2N-3)} \rangle_t$, $\langle \delta x_j^{(2N-3)}/p_{xj} \rangle_t$, and $\langle \delta y_j^{(2N-3)}/p_{yj} \rangle_t$ to sinusoidal functions multiplied by constants, as functions of $1/\sqrt{2mE/N}$. Here we used a quasi-one-dimensional system of 50 hard disks with (H,P) boundary conditions, and calculated the amplitudes $|\alpha_1'|$ and $|\tilde{\alpha}_1'|$ for different total energies E. In Fig. 6, we fitted the amplitude $|\tilde{\alpha}_1'|$ for the mode $\langle \delta x_j^{(2N-3)} \rangle_t$ (circles) to a constant function $|\tilde{\alpha}_1'| = \xi$ (the broken line) with a fitting parameter value $\xi \approx 0.179$, and the solid line is given by the linear function $\xi/\sqrt{2mE/N}$ of $1/\sqrt{2mE/N}$ using this value of ξ. The amplitudes $|\alpha_1'|$ for the modes $\langle \delta x_j^{(2N-3)}/p_{xj} \rangle_t$ (triangles) and $\langle \delta y_j^{(2N-3)}/p_{yj} \rangle_t$ (squares) are reasonably on this linear line $\xi/\sqrt{2mE/N}$, and these results support the relation Eq. (4), and also suggest that the amplitude $|\tilde{\alpha}_k'|$ for the mode $\langle \delta x_j^{(2N-3)} \rangle_t$ is independent of $1/\sqrt{2mE/N}$. The amplitudes $|\alpha_k'|$ for $\langle \delta x_j^{(2N-3)}/p_{xj} \rangle_t$ (triangles) and $\langle \delta y_j^{(2N-3)}/p_{yj} \rangle_t$ (squares) in Fig. 6 almost coincide with each other, and this gives support to the claim that the coefficients α_k' on the x component and the y component of the first term on the right-hand side of Eq. (2) coincide.

In the above argument, we assumed the normalizability of the spatial part only of the Lyapunov vectors. This can be justified by the fact that, as shown in Sec. III F, the spatial part and momentum part of Lyapunov vector modes show almost the same mode structure, so each of them should be independently normalizable.

E. Spatial node structures of the Lyapunov modes and reflections at hard walls

The spatial node structure of the Lyapunov modes can be explained using the collision rule for particles with hard walls. For (H,P) boundary conditions, the particle collisions with the hard walls in the x direction cause a change in the sign of the x component of the momentum with the remaining components of the phase-space vector unchanged,

$$x_j \to x_j, \tag{7}$$

$$y_j \to y_j, \tag{8}$$

$$p_{xj} \to -p_{xj}, \tag{9}$$

$$p_{yj} \to p_{yj}. \tag{10}$$

Similarly, in this type of collision, the x components of the Lyapunov vector change their signs while the remaining components are unchanged,

$$\delta x_j \to -\delta x_j, \tag{11}$$

$$\delta y_j \to \delta y_j, \tag{12}$$

$$\delta p_{xj} \to -\delta p_{xj}, \tag{13}$$

$$\delta p_{yj} \to \delta p_{yj}. \tag{14}$$

Note that the x components of Lyapunov vector δx_j change sign as well as δp_{xj}, which is different from the phase-space vector.

The important point is that a system with hard-wall boundaries is equivalent to an infinite system generated by reflecting the positions and velocities of all particles (in the hard wall) and by changing the signs of all x components of the Lyapunov vectors at the hard wall. That is explicitly incorporating the reflection symmetries for the phase-space vector and the Lyapunov vector at hard walls. If the modes of the entire system are smoothly connected sinusoidal functions at the hard walls, then this condition requires that the mode for the quantity δx_j has a node at a hard wall, because it changes sign there. On the other hand, the quantities $\delta x_j/p_{xj}$ and $\delta y_j/p_{yj}$ do not change their signs at hard walls, so these modes should have antinodes at hard walls. These results explain the spatial node structures shown in Fig. 5. The spatial node structure of the stationary Lyapunov modes in δy_j corresponding to the one-point steps can be explained

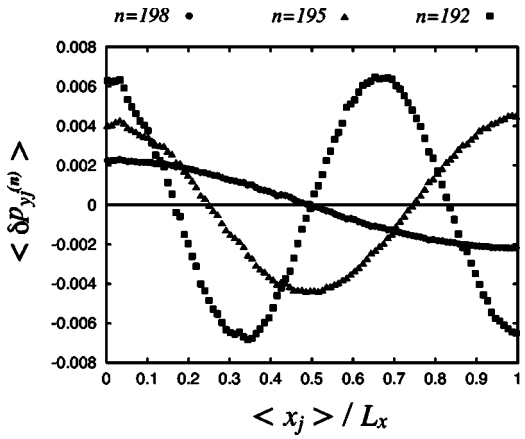

FIG. 7. Global time averages $\langle \delta p_{yj}^{(n)} \rangle$ for the Lyapunov exponents corresponding to the first, second, and third one-point step of the Lyapunov spectrum [$n=198$ (circles), 195 (triangles), and 192 (squares)] as functions of the normalized global time average $\langle x_j \rangle / L_x$ of the position of the jth particle.

in this way. Because δy_j varies sinusoidally and must satisfy the reflection symmetry, it must be either a node (if the sign changes) or an antinode (if the sign is invariant). Hence, in this case the Lyapunov mode in δy_j should have an antinode at the hard walls.

F. Lyapunov modes in momentum components of Lyapunov vectors

So far, we have discussed only the spatial components of the Lyapunov vectors. In this subsection, we discuss briefly the Lyapunov modes appearing in the momentum parts of Lyapunov vectors.

One of the few differences between spatial and momentum components of Lyapunov vectors is that the amplitudes of the momentum components are often much smaller than those of the corresponding spatial components [11]. This makes Lyapunov modes for the momentum parts of the Lyapunov vectors less clear than the corresponding spatial components. However, basically the structure of the Lyapunov mode for the momentum part of the Lyapunov vector is quite similar to the corresponding spatial component. For this reason, in this subsection we omit a detailed discussion of the phase relations of multiple Lyapunov modes for the momentum parts of Lyapunov vectors, and just show that there are certain mode structures in the momentum components of Lyapunov vectors corresponding to the Lyapunov steps.

Figure 7 shows the mode structure of $\delta p_{yj}^{(n)}$ corresponding to the first three one-point steps ($n=198$, 195, and 192) as functions of the normalized particle positions for $N=100$. This structure is stationary in time, so we took their global time average over $200N$ collisions, using the notation $\langle \cdots \rangle$ for this global time average without the suffix t. These modes are similar to the ones for the corresponding spatial part $\delta y_j^{(n)}$ discussed in Sec. III B.

Figure 8 shows contour plots of time-oscillating Lyapunov modes for $\langle \delta p_{xj}^{(197)} \rangle_t$, $\langle \delta p_{xj}^{(197)} / p_{xj} \rangle_t$, and $\langle \delta p_{yj}^{(197)} / p_{yj} \rangle_t$ as functions of the collision number n_t and the normalized local time average $\langle x_j \rangle_t / L_x$ in the first two-point step. We used the same collision number interval [535200, 569600] in Fig. 8 as in Fig. 5. The mode structures in Figs. 8(a)–8(c) are almost the same as Figs. 5(a), 5(c), and 5(e) for the corresponding spatial components $\langle \delta x_j^{(197)} \rangle_t$, $\langle \delta x_j^{(197)} / p_{xj} \rangle_t$, and $\langle \delta y_j^{(197)} / p_{yj} \rangle_t$, respectively, although their oscillating amplitudes are much smaller than those of the corresponding spatial components.

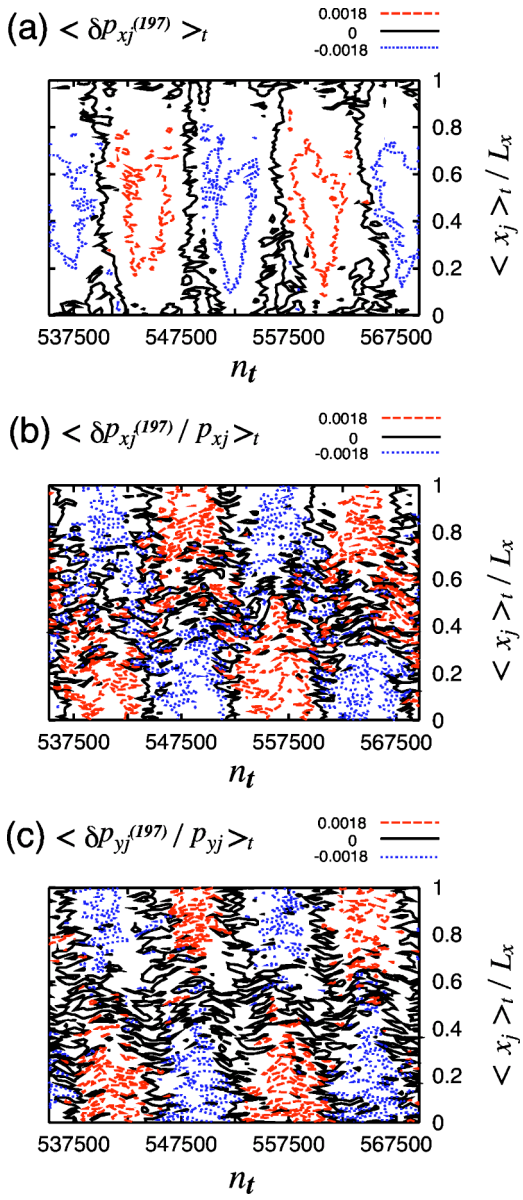

FIG. 8. (Color online) Contour plots of the local time averages of $\langle \delta p_{xj} \rangle_t$, $\langle \delta p_{xj} / p_{xj} \rangle_t$, and $\langle \delta p_{yj} / p_{yj} \rangle_t$ for the first exponent (197) of the first two-point step as a function of the collision number n_t and the normalized position of the jth particle (in the collision number interval [535200, 569600]). The dotted lines, solid lines, and broken lines are contour lines at the levels −0.0018, 0, and +0.0018, respectively.

The spatial mode structures of the momentum components of Lyapunov vectors are explained by the same reflec-

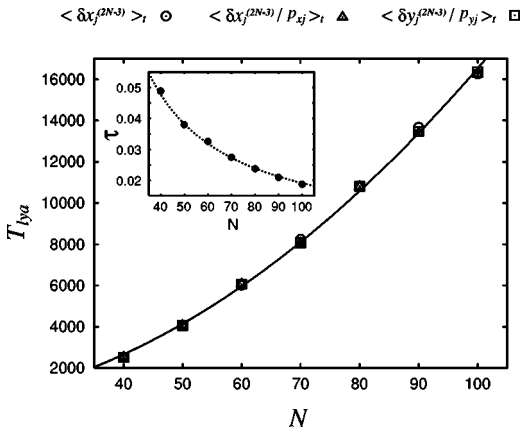

FIG. 9. Particle number (N) dependence of the period T_{Lya} of the time oscillations of $\langle \delta x_j^{(2N-3)} \rangle_t$ (circles), $\langle \delta x_j^{(2N-3)} / p_{xj} \rangle_t$ (triangles), and $\langle \delta y_j^{(2N-3)} / p_{yj} \rangle_t$ (squares) in the quasi-one-dimensional system with (H,P) boundary condition. The data are fitted to the function $T_{\mathrm{Lya}} = \alpha + \beta N^2$ with the fitting parameters α and β. The inset: Particle number dependence of the mean free time τ with a fitting function $\tau = \gamma / N$ with the fitting parameter γ.

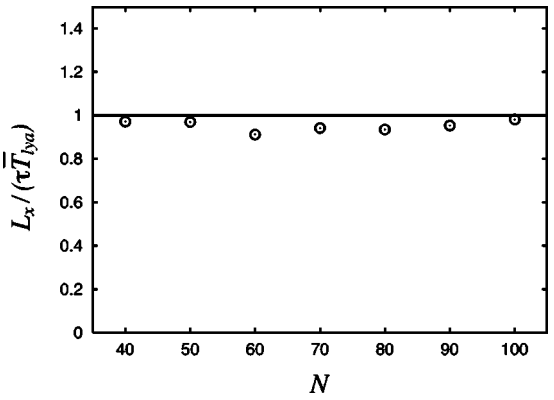

FIG. 10. The quantity $L_x / (\tau \overline{T}_{\mathrm{Lya}})$ as a function of the number of particles N. Here, $\overline{T}_{\mathrm{Lya}}$ is the collision number interval given by the average of the three collision number intervals T_{Lya} for time oscillations of the Lyapunov vector components $\langle \delta x_j^{(2N-3)} \rangle_t$, $\langle \delta x_j^{(2N-3)} / p_{xj} \rangle_t$, and $\langle \delta y_j^{(2N-3)} / p_{yj} \rangle_t$ in the first two-point step of the Lyapunov spectra. The line is given by $L_x / (\tau \overline{T}_{\mathrm{Lya}}) = 1$, which is the x component of the thermal velocity $\sqrt{E/(mN)}$.

tion property at hard walls, which was discussed in the previous Sec. III E.

G. Particle number dependence of the oscillating periods

In Sec. III C, we showed that the quantities $\langle \delta x_j^{(n)} \rangle_t$, $\langle \delta x_j^{(n)} / p_{xj} \rangle_t$, and $\langle \delta y_j^{(n)} / p_{yj} \rangle_t$ corresponding to the two-point Lyapunov steps show time-oscillating behavior. Now we consider how the time-oscillating period of those Lyapunov modes depends on the number of particles N at fixed density.

We evaluate the collision number interval for the time oscillation of Lyapunov modes as follows. As shown in the proceeding Sec. III C, the Lyapunov modes related to the quantity $\langle \delta x_j^{(n)} \rangle_t$ (the quantities $\langle \delta x_j^{(n)} / p_{xj} \rangle_t$ and $\langle \delta y_j^{(n)} / p_{yj} \rangle_t$) have an antinode in the middle (at the end) of the system in the x direction ($n = 2N-3$ and $2N-4$) for the (H,P) boundary condition. Using this property, we took six data points for the quantity $\langle \delta x_j^{(n)} \rangle_t$ (the quantities $\langle \delta x_j^{(n)} / p_{xj} \rangle_t$ and $\langle \delta y_j^{(n)} / p_{yj} \rangle_t$) ($n = 2N-3$) in the middle (at the end) of the system with the (H,P) boundary condition. These data are fitted to a sinusoidal function $a \sin\{(2\pi n_t / T_{\mathrm{Lya}}) + b\}$ of n_t with fitting parameters a, b, and T_{Lya}, which leads to a numerical estimation of the period T_{Lya} of the time oscillation of the Lyapunov modes. The collision number interval T_{Lya} can be translated into a real time interval by multiplying by the mean free time τ.

Figure 9 is the graph of the period T_{Lya} of the time oscillations of $\langle \delta x_j^{(197)} \rangle_t$ (circles), $\langle \delta x_j^{(197)} / p_{xj} \rangle_t$ (triangles), and $\langle \delta y_j^{(197)} / p_{yj} \rangle_t$ (squares) in the quasi-one-dimensional system with the (H,P) boundary condition, as functions of the number of particles N. Spatial and temporal behavior of these quantities has already been shown in Figs. 4(a), 4(b), and 4(d) for $N = 100$. Figure 9 shows that the three time oscillations associated with $\langle \delta x_j^{(197)} \rangle_t$, $\langle \delta x_j^{(197)} / p_{xj} \rangle_t$, and $\langle \delta y_j^{(197)} / p_{yj} \rangle_t$ all have the same period. In Fig. 9, the data are fitted to a quadratic function $T_{\mathrm{Lya}} = \alpha + \beta N^2$ with the fitting parameter values $\alpha \approx 17.9$ and $\beta \approx 1.65$. The inset to this figure shows the mean free time τ as a function of the number of particles N. The N dependence of τ is nicely fitted to the function $\tau = \gamma / N$, where $\gamma \approx 1.91$. Noting that the period, in real time, is approximately given by τT_{Lya}, these results suggest that the period of the Lyapunov modes is almost proportional to the number of particles N.

Now, we investigate the time-oscillating period of the Lyapunov modes in a different way. Figure 10 shows the quantity $L_x / (\tau \overline{T}_{\mathrm{Lya}})$ using the system length L_x, the mean free time τ, and the averaged time-oscillating periods $\tau \overline{T}_{\mathrm{Lya}}$ of the Lyapunov modes in $\langle \delta x_j^{(2N-3)} \rangle_t$, $\langle \delta x_j^{(2N-3)} / p_{xj} \rangle_t$, and $\langle \delta y_j^{(2N-3)} / p_{yj} \rangle_t$ in the first two-point step of the Lyapunov spectrum. This figure suggests that this quantity is almost 1, that is, independent of the particle number N, therefore equal to the x component of the thermal velocity $\sqrt{E/(mN)}$.

IV. AUTOCORRELATION FUNCTIONS

In this section, we discuss another property of the quasi-one-dimensional system, namely, the time-oscillation behavior of the momentum autocorrelation function. This is a typical measure of the collective behavior of many-particle systems. We connect this behavior with the time-oscillating behavior of the Lyapunov modes, suggesting that the time oscillation of the Lyapunov modes can also be regarded as a collective mode.

We calculate the autocorrelation functions $C_\eta(t)$ for the η component ($\eta = x$ or y) of the momentum using the normalized expression $C_\eta(t) \equiv \tilde{C}_\eta(t) / \tilde{C}_\eta(0)$, in which $\tilde{C}_\eta(t)$ is defined by

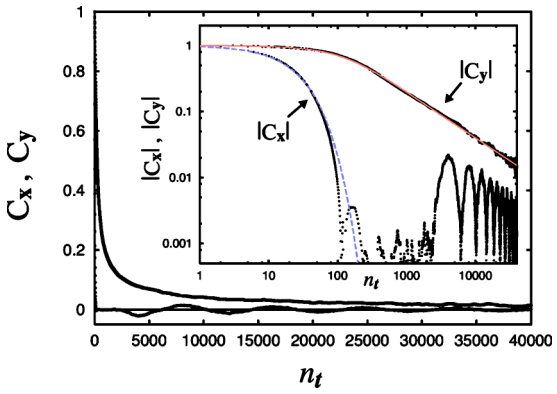

FIG. 11. (Color online) The autocorrelation function C_x and C_y for the x and y components of momentum, respectively, as functions of the collision number n_t. Main figure: Linear-linear plots of C_x and C_y as functions of n_t. The inset: Log-log plots of the absolute values $|C_x|$ and $|C_y|$ as functions of n_t. Here, the broken line is a fit of the graph of $|C_x|$ to an exponential function, and the line is a fit of the graph of $|C_y|$ to a κ-exponential function [defined by Eq. (18)].

$$\tilde{C}_\eta(t) \equiv \lim_{T\to+\infty} \frac{1}{(N_2 - N_1 + 1)T} \sum_{j=N_1}^{N_2} \int_0^T ds p_{\eta j}(s+t) p_{\eta j}(s). \tag{15}$$

Equation (15) includes a time average and an average over some of the particles (from the N_1th particle to the N_2th particle) in the middle of the system. (Note that the particles are numbered $1,2,\ldots,N$ from left to right in the system, as shown in Fig. 1.) In actual calculations, we choose $N_1=[(N+1)/2]-5$ and $N_2=[(N+1)/2]+5$ with $[x]$ as the integer part of the real number x. This means that we take into account only 11 particles in the middle of the system in the calculation of the autocorrelation function $C_\eta(t)$. (In this paper, we consider the case $N \geqslant 40 > 11$.) It should be noted that using the (H,P) boundary condition, the autocorrelation function for particles near hard walls is different from the ones for particles in the middle of the system, as discussed in Appendix A. Especially, the momentum autocorrelation function of particles near hard walls does not show clear time-oscillating behavior. To get the clearest time-oscillating behavior for the autocorrelation function $C_\eta(t)$ and to get fewer hard-wall boundary condition effects, we exclude the autocorrelation functions of particles near hard walls in the calculation of $C_\eta(t)$.

If the system is ergodic, the value of the autocorrelation function (15) will be independent of the initial condition. To get the results for the autocorrelation function, in this section we take a time average of the autocorrelation function over more than 2×10^6 collisions. In the figures, the autocorrelation functions are shown as functions of the collision number n_t.

A. Momentum autocorrelation functions and their direction dependence

Figure 11 contains the momentum autocorrelation functions C_x and C_y for the momentum components in the x and y directions, respectively, as a function of the collision number n_t in the quasi-one-dimensional system with $N=100$ and (H,P) boundary condition. The main figure in Fig. 11 is a linear-linear plot of the autocorrelation functions C_x and C_y, while its inset is a log-log plot of the graph of the absolute values $|C_x|$ and $|C_y|$. In this system, the mean free time is given by $\tau \approx 0.0188$. From Fig. 11 it is clear that the momentum autocorrelation function has a strong direction dependence and shows a time-oscillating behavior in C_x.

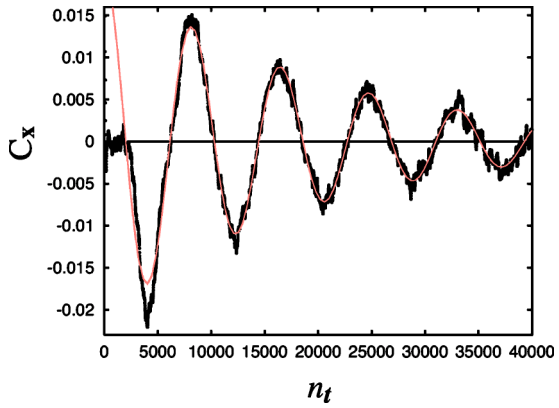

FIG. 12. (Color online) The time-oscillating part of autocorrelation function C_x for the x component of momentum as functions of the collision number n_t. Here, the line is the fit to the product of a sinusoidal and an exponential function.

Initially, the autocorrelation function C_x decays exponentially with time. To show this point, in the inset to Fig. 11 we fitted the initial part of $|C_x|$ to an exponential function

$$G_1(n_t) \equiv \exp\{-\alpha' n_t\}, \tag{16}$$

with the fitting parameter value $\alpha' \approx 0.0385$.

The significant point about the autocorrelation function C_x is its time-oscillating behavior. To show this behavior explicitly, we show Fig. 12 as an enlarged graph of the time-oscillating part of C_x, which is already shown in Fig. 11. This time oscillation accompanies a time decay, so we fitted this graph to the product of a sinusoidal and an exponential function $G_2(n_t)$, namely,

$$G_2(n_t) \equiv \mathcal{A} e^{-\beta' n_t} \sin\left(\frac{2\pi}{T_{acf}} n_t + \xi\right), \tag{17}$$

with fitting parameters $\mathcal{A}$, β', T_{acf}, and ξ. The time-oscillating part of the autocorrelation function C_x is nicely fitted to this function with the parameter values $\mathcal{A} \approx 0.0209$, $\beta' \approx 5.17\times10^{-5}$, $T_{acf} \approx 8.29\times10^3$, and $\xi \approx 1.62$. This also gives us a way of numerically evaluating the oscillation period T_{acf} of the autocorrelation function C_x. We note that the quasi-one-dimensional system shows a much clearer time-oscillating behavior of the momentum autocorrelation function than a fully two- (or three-) dimensional system. One may ask whether the damping behavior of the envelope of time oscillation of C_x is best fitted to a power-law function, like the slow damping of the long time behavior of C_y, rather than to an exponential function as assumed in Eq. (17). (Ac-

tually the data in Fig. 12 are not sufficient to decide between exponential and power decay.) This point is discussed further in Appendix B.

On the other hand, the autocorrelation function C_y shows a different behavior from C_x. This comes from the specific shape of the system and the boundary conditions. As shown in Fig. 11, the damping of the momentum autocorrelation function C_y is much slower than for C_x. This is explained by the fact that in this quasi-one-dimensional system, a collision where the vector separation between particle centers points purely in the y direction (either positive or negative) cannot occur, because the periodic images of the particle prevent other particles approaching in this direction. This preferential collision geometry leads to a preference for a larger change in the x component of momentum at collisions than the y component of momentum, and hence a faster decay of the C_x correlation function. In the inset to Fig. 11, the graph of the autocorrelation function for the C_y is fitted to the "κ-exponential function" $F_\kappa(t)$, which is defined by

$$F_\kappa(t) \equiv [\sqrt{1+(\alpha''\kappa t)^2} - \alpha''\kappa t]^{1/\kappa}, \tag{18}$$

with $\alpha''\kappa t \geqslant 0$ and fitting parameters α'' and κ. In the collision number region shown in Fig. 11, the autocorrelation function C_y is positive, so this fitting can be for C_y as well as for $|C_y|$. From the definition, in the limit as $\kappa=0$ the function $F_\kappa(t)$ becomes the exponential function: $\lim_{\kappa\to 0} F_\kappa(t)=\exp\{-\alpha''t\}$, noting $F_\kappa(0)=1$ and $\partial F_\kappa(t)/\partial t = -\alpha'' F_\kappa(t)/\sqrt{1+(\alpha''\kappa t)^2}$, so this function is a one-parameter deformation of the exponential function [45]. The important properties of this function are that it is approximated by an exponential function at small $\alpha''\kappa t$ and is approximately a power function at large $\alpha''\kappa t$ [by direct expansion of Eq. (18)],

$$F_\kappa(t) \sim \begin{cases} e^{-\alpha'' t} & \text{in } \alpha''\kappa t \ll 1 \\ (2\kappa\alpha'' t)^{-1/\kappa} & \text{in } \alpha''\kappa t \gg 1. \end{cases} \tag{19}$$

Fitting the numerical data for the autocorrelation function C_y to the κ-exponential function $F_\kappa(n_t)$ with parameter values $\alpha'' \approx 0.00\,358$ and $\kappa \approx 1.44$ is very satisfactory, and this implies that this autocorrelation function decays exponentially initially (like C_x), and decays as a power function after that, at least in the time scale shown in Fig. 11. (This does not mean that the autocorrelation function C_y decays as a κ-exponential function in any time scale. See Appendix B about C_y at much longer time scales than shown in Fig. 11.)

B. Particle number dependence of the autocorrelation function and its relation to the time oscillation of the Lyapunov modes

We have shown the two kinds of time-oscillation behaviors in the quasi-one-dimensional system: one for the Lyapunov mode and another for the momentum autocorrelation function. Now we show numerical evidence to connect these two behaviors.

Figure 13 is the graph of the largest time-oscillating period $\overline{T}_{\rm Lya}$ of the Lyapunov modes as a function of the time-oscillating period T_{acf} of the momentum autocorrelation function C_x. Here, the time-oscillating periods are calculated for $N=40,50,60,\ldots,100$ at constant density, and the time-oscillating periods $\overline{T}_{\rm Lya}$ are calculated as the average of the collision number interval $T_{\rm Lya}$ for time oscillations of the Lyapunov vector components $\langle \delta x_j^{(2N-3)}\rangle_t$, $\langle \delta x_j^{(2N-3)}/p_{xj}\rangle_t$, and $\langle \delta y_j^{(2N-3)}/p_{yj}\rangle_t$ in the first two-point step of the Lyapunov spectra. (As shown in Sec. III G, these three oscillating periods $T_{\rm Lya}$ of the Lyapunov modes take almost the same values.) In Fig. 13, we also show the line given by the function $\overline{T}_{\rm Lya}=2T_{acf}$. The numerical data for the time oscillations in Fig. 13 are nicely fitted to this function, and suggest the relation

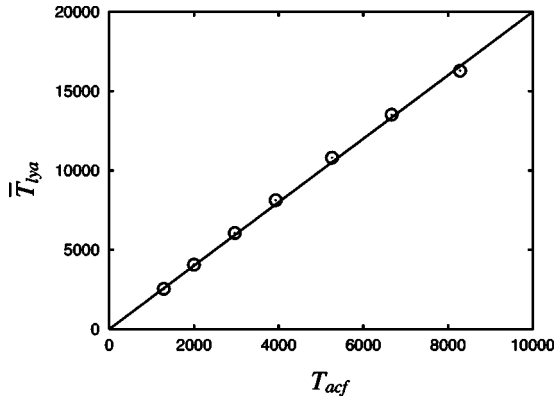

FIG. 13. The period $\overline{T}_{\rm Lya}$ (in collision numbers) of the time oscillation of the Lyapunov mode as a function of the period of time oscillation of the longitudinal momentum autocorrelation function T_{acf}. Data points are obtained from numerical calculation of the quasi-one-dimensional system with (H,P) boundary condition for different numbers of particles $N=40,50,60,\ldots,100$ at constant density. The line is given by the function $\overline{T}_{\rm Lya}=2T_{acf}$.

$$T_{\rm Lya} \approx 2T_{acf}. \tag{20}$$

This is the main result of this paper. The result given in Fig. 13 supports the particle number (N) independence of the relation (20) with a fixed density, but this relation is also independent of density changes. The density independence of the relation (20) comes from the fact that the time-oscillating periods T_{acf} and $T_{\rm Lya}$ in mean free time unit do not almost depend on the particle density.

In Table I, we summarize not only the values of the time-oscillating periods $\overline{T}_{\rm Lya}\tau$ and $T_{acf}\tau$ of the Lyapunov modes and the momentum autocorrelation function in real time, but also the data for the N dependences of the damping properties of the autocorrelation functions C_x and C_y. They include the mean free time τ, the exponential damping times τ/α' and τ/β' (for C_x) and τ/α'' (for C_y), and the power $1/\kappa$ of the damping of C_y at long time. Here, values of α', β', and T_{acf} (α'' and κ) are derived by fitting the autocorrelation function C_x (C_y) to Eqs. (16) and (17) [Eq. (18)]. From this table it is clear that the exponential damping times τ/α' and τ/α'', and the power $1/\kappa$, are almost independent of the particle number N. On the other hand, the exponential damping time τ/β' of the time oscillation of the autocorrelation C_x increases as N increases. (We have already discussed the N

TABLE I. Time-oscillating periods and decay rates for the Lyapunov modes and the momentum autocorrelation functions. Here, N is the number of particles, τ is the mean free time, and $\overline{T}_{\mathrm{Lya}}$ is the collision number interval given by taking an average of the three collision number intervals T_{Lya} for the time oscillations of the Lyapunov vector components $\langle \delta x_j \rangle_t$, $\langle \delta x_j / p_{xj} \rangle_t$, and $\langle \delta y_j / p_{yj} \rangle_t$ corresponding to the first two-point step. The parameter α' is given by fitting the beginning of the longitudinal momentum autocorrelation function C_x as a function of the collision number n_t to an exponential function $C_x = \exp\{-\alpha' n_t\}$. The parameters β' and T_{acf} are given by fitting the time-oscillating part of the same function C_x to the function $C_x = \mathcal{A} \exp\{-\beta' n_t\} \sin[(2\pi / T_{acf}) n_t + \xi]$. The parameters α'' and κ are given by fitting the transverse momentum autocorrelation function C_y as a function of the collision number n_t to the κ-exponential function in Eq. (18).

		Lyapunov mode	C_x			C_y	
N	τ	$\overline{T}_{\mathrm{Lya}}\tau$	τ/α'	τ/β'	$T_{acf}\tau$	τ/α''	$1/\kappa$
40	0.0489	124	0.49	74	63	5.3	0.73
50	0.0380	154	0.48	103	76	5.3	0.72
60	0.0326	197	0.51	156	97	5.4	0.68
70	0.0275	223	0.49	196	108	5.3	0.61
80	0.0238	257	0.49	205	125	4.7	0.58
90	0.0210	283	0.49	252	140	4.9	0.62
100	0.0188	306	0.49	363	156	5.3	0.69

dependence of the mean free time τ in Sec. III G.)

C. Boundary condition effects

So far, we have concentrated on the quasi-one-dimensional system with hard-wall boundary conditions in the x direction and periodic boundary conditions in the y direction, namely, the (H,P) boundary condition, for technical convenience in the analysis of the Lyapunov modes. On the other hand, in Ref. [18] we have already discussed and compared Lyapunov steps and modes in the different boundary conditions: the purely periodic boundary conditions (P,P), the purely hard-wall boundary conditions (H,H), and periodic boundary conditions in the x direction and hard-wall boundary conditions in the y direction (P,H) as well as the boundary condition (H,P). In this section, we carry out a similar discussion for the momentum autocorrelation functions C_x in these different boundary conditions. Figure 14 contains schematic illustrations of these boundary conditions.

For meaningful comparisons between the different boundary conditions, we use the same mass m and radius R for the particles, and the same number of particles ($N=50$). Using the set of the lengths (L_x, L_y) to define the size of the system in the x and y directions for (H,P) boundary conditions, we use $(L_x - 2R, L_y)$ for (P,P) boundary conditions, $(L_x - 2R, L_y + 2R)$ for (P,H) boundary conditions, and $(L_x, L_y + 2R)$ for (H,H) boundary conditions. This gives the same effective area for particles to move in each of the four systems. This also means that the mean free time τ in these four types of boundary conditions will be the same (concrete numerical values of τ are given in Table II).

Figure 15 shows the autocorrelation functions C_x for the x component of the momenta in quasi-one-dimensional systems consisting of 50 hard disks with boundary conditions (P,P), (P,H), (H,P), and (H,H) as functions of the collision number n_t. Here, Fig. 15(a) is the initial part of the autocorrelation functions C_x, and is given as a linear-log plot to show their exponential decay as straight lines. In this figure, the fits to the exponential function Eq. (16) with the fitting parameter α' are given for the cases (P,P) and (H,P) and the cases (P,H) and (H,H) separately. The dotted line is the fit for the cases (P,P) and (H,P) with the fitting parameter values $\alpha' \approx 0.0765$, and the broken line is for the cases (P,H) and (H,H) with the fitting parameter values $\alpha' \approx 0.0597$. Figure 15(b) is the time-oscillating part of C_x in the four different boundary conditions. In this figure, each autocorrelation function is fitted to the function (17) with the fitting param-

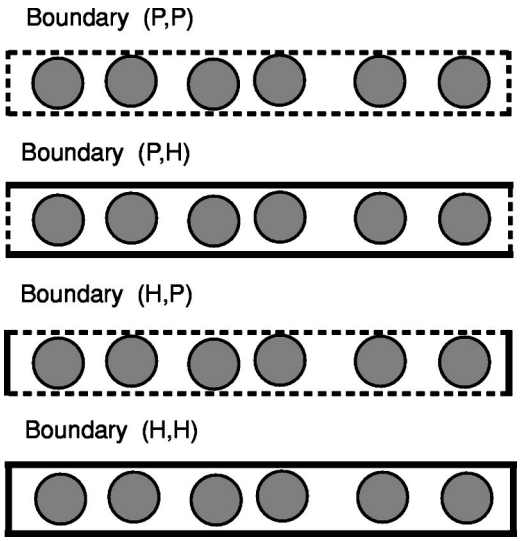

FIG. 14. Schematic illustrations of the four boundary conditions (P,P), (P,H), (H,P), and (H,H) used in quasi-one-dimensional systems. Here, (P,P) is the purely periodic boundary conditions, (P,H) is periodic boundary conditions in the x direction and hard-wall boundary conditions in the y direction, (H,P) is hard-wall boundary conditions in the x direction and periodic boundary conditions in the y direction, and (H,H) is the purely hard-wall boundary conditions. The dashed lines and the solid lines on the boundaries represent periodic boundary conditions and hard-wall boundary conditions, respectively.

TABLE II. The mean free time τ, the time-oscillating time period $T_{acf}\tau$ of the longitudinal momentum autocorrelation function C_x, and the average of the longest time-oscillating time period $\overline{T}_{\mathrm{Lya}}\tau$ of the Lyapunov vector, for the different boundary conditions (P,P), (P,H), (H,P), and (H,H) in a quasi-one-dimensional system of 50 hard disks. $\overline{T}_{\mathrm{Lya}}$ is the average over three collision number intervals of T_{Lya}. Here, T_{Lya} is the average of the time oscillations of the three components $\langle \delta x_j^{(k)} \rangle_t$, $\langle \delta x_j^{(k)}/p_{xj} \rangle_t$, and $\langle \delta y_j^{(k)}/p_{yj} \rangle_t$ for the first Lyapunov step which has time-oscillating Lyapunov modes [$k=2N-5$ for (P,P), $k=2N-2$ for (P,H), $k=2N-3$ for (H,P), and $k=2N-1$ for (H,H)].

Boundary	τ	$T_{acf}\tau$	$\overline{T}_{\mathrm{Lya}}\tau$
(P,P)	0.0369	37.4	77.0
(P,H)	0.0371	45.8	91.4
(H,P)	0.0380	77.3	154.5
(H,H)	0.0383	96.8	194.5

eters $\mathcal{A}$, β', T_{acf}, and ξ. The values of these fitting parameters are $(\mathcal{A},\beta',T_{acf},\xi) \approx (0.0422, 0.001\,08, 1.00 \times 10^3, 1.37)$ for (P,P), $(\mathcal{A},\beta',T_{acf},\xi) \approx (0.0447, 0.000\,803, 1.24\times 10^3, 1.33)$ for (P,H), $(\mathcal{A},\beta',T_{acf},\xi) \approx (0.0398, 0.000\,369, 2.04\times 10^3, 1.56)$ for (H,P), and $(\mathcal{A},\beta',T_{acf},\xi) \approx (0.0403, 0.000\,246, 2.53 \times 10^3, 1.56)$ for (H,H).

Figure 15(a) shows that the boundary condition in the y direction has a strong effect on the autocorrelation function C_x even at short time. In the cases (P,P) and (H,P), the autocorrelation function C_x shows faster exponential decay than for (P,H) and (H,H), as shown in the difference of the value of the fitting parameter α' for the exponential fitting function Eq. (16). In the collision number region shown in Fig. 15(a), the effects of the boundary conditions in the x direction in the autocorrelation function C_x appear after showing their initial exponential decays, and the autocorrelation function C_x for (P,P) [and (P,H)] decays faster than C_x for (H,P) [and (H,H)].

On the other hand, Fig. 15(b) shows that in all the boundary conditions, the autocorrelation functions C_x show time oscillations, but with different oscillating periods T_{acf}. In this figure we can recognize that the second peak of C_x for (P,P) coincides with the first peak of C_x for (H,P). A similar coincidence appears in the second peak of C_x for (P,H) and the first peak of C_x in (H,H). Actually, the fitting parameter value of T_{acf} for (P,P) [(P,H)] is approximately half the value of T_{acf} for (H,P) [(H,H)]. This can be simply explained by the fact that when replacing the periodic boundary conditions with the hard-wall boundary conditions, twice the time is required for a particle perturbation to come back to the same position.

Finally, we show the relation between the time-oscillating periods of the Lyapunov mode and the momentum autocorrelation function for different boundary conditions. In Table II, we summarize the mean free time τ, the time-oscillating time period $T_{acf}\tau$ of the momentum autocorrelation function C_x, and the time-oscillating time period $\overline{T}_{\mathrm{Lya}}\tau$ of the largest Lyapunov mode for the four kinds of boundary conditions

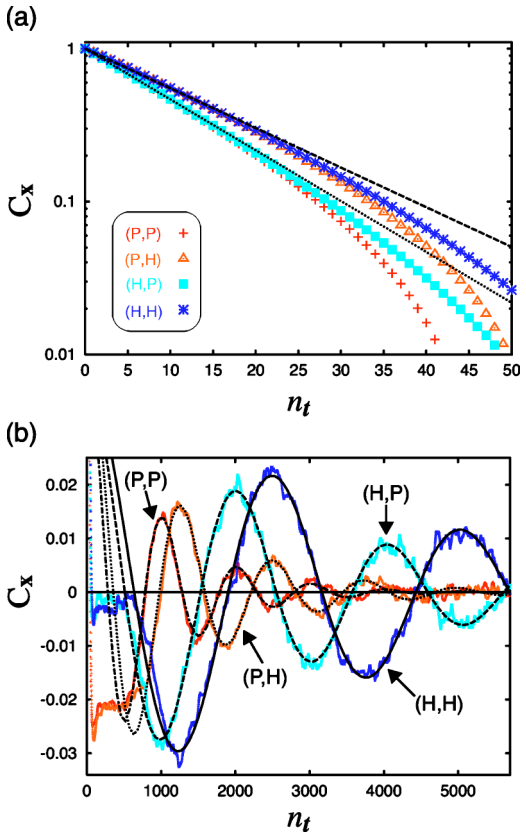

FIG. 15. (Color online) C_x as a function of the collision number n_t for each different boundary condition (P,P), (P,H), (H,P), and (H,H). The systems are quasi-one-dimensional systems consisting of 50 hard disks. We observe (a) exponential decay region in the initial damping of the autocorrelation function C_x as a linear-log plot. The dotted line and the broken line are the fits for the cases (P,P) and (H,P) and the cases (P,H) and (H,H) to exponential functions, respectively. (b) Time-oscillating region of the autocorrelation functions C_x as a linear-linear plot. The four graphs of the autocorrelation functions C_x are fitted to the functions $C_x=\mathcal{A}\exp\{-\beta' n_t\}\sin\{(2\pi/T_{acf})n_t+\xi\}$ with the fitting parameters $\mathcal{A}$, β', T_{acf}, and ξ.

(P,P), (P,H), (H,P), and (H,H). Here, the period $\overline{T}_{\mathrm{Lya}}$ is evaluated as the arithmetic average of the collision number intervals T_{Lya} for the quantities $\langle \delta x_j^{(k)} \rangle_t$, $\langle \delta x_j^{(k)}/p_{xj} \rangle_t$, and $\langle \delta y_j^{(k)}/p_{yj} \rangle_t$. The Lyapunov indices k are chosen from the Lyapunov exponents in the first Lyapunov step which has time-oscillating behavior of its Lyapunov modes. Our result supports the conjecture that the relation (20) is satisfied for all boundary conditions (P,P), (P,H), (H,P), and (H,H).

D. An explanation for the relation of time-oscillation periods of the Lyapunov mode and the momentum autocorrelation function

As we have shown, the relation $T_{\mathrm{Lya}}=2T_{acf}$ [Eq. (20)] between the largest time-oscillating period T_{Lya} of the Lyapunov modes and the time-oscillating period T_{acf} of the momentum autocorrelation function is independent of the number of particles N and the boundary conditions. In this

subsection, we discuss a possible explanation for this relation, which is a physical argument rather than a strict mathematical proof.

First, we consider a momentum component $\tilde{p}_x(t)$, like the x component of the momentum in the quasi-one-dimensional system, which shows a time-oscillating behavior in its autocorrelation function with a frequency ω_{acf},

$$\overline{\tilde{p}_x(t)^* \tilde{p}_x(0)} \sim \phi(t) e^{i\omega_{acf} t}, \tag{21}$$

where we use the notation $\overline{X(t)^* X(0)}$ for the autocorrelation function for any complex quantity $X(t)$ with complex conjugate $X(t)^*$. Here $\phi(t)$ is the damping envelope of the autocorrelation function $\overline{\tilde{p}_x(t)^* \tilde{p}_x(0)}$, which can be an exponential decay, $\phi(t) \sim \exp\{-\tilde{\alpha} t\}$, with a positive constant $\tilde{\alpha}$ (see Appendix B).

Next, we consider the time-dependent Lyapunov mode with the largest time-oscillating period, and we represent its momentum proportional and time-oscillating term in the Lyapunov vector, like the x component of the first terms on the right-hand sides of Eqs. (2) and (3), as

$$\delta\tilde{q}_x \sim \psi_1(t) \tilde{p}_x(t) e^{i\omega_{\mathrm{Lya}} t} \tag{22}$$

with a frequency ω_{Lya}, where $\psi_1(t)$ is the envelope function of the amplitude of $\delta\tilde{q}_x$, and it may show an exponential divergence (or contraction) following the corresponding Lyapunov exponent. Now, we assume that if the quantity $\delta\tilde{q}_x$ oscillates persistently in time, then its autocorrelation function $\overline{\delta\tilde{q}_x(t)^* \delta\tilde{q}_x(0)}$ should oscillate in time with the same frequency ω_{Lya}, namely,

$$\overline{\delta\tilde{q}_x(t)^* \delta\tilde{q}_x(0)} \sim \psi_2(t) e^{i\omega_{\mathrm{Lya}} t} \tag{23}$$

with a new envelope function $\psi_2(t)$.

It follows from Eqs. (21)–(23) that

$$\begin{aligned} \psi_2(t) e^{i\omega_{\mathrm{Lya}} t} &\sim \psi_1(t)^* \psi_1(0) \overline{\tilde{p}_x(t)^* \tilde{p}_x(0)} e^{-i\omega_{\mathrm{Lya}} t} \\ &\sim \psi_1(t)^* \psi_1(0) \phi(t) e^{i(\omega_{acf} - \omega_{\mathrm{Lya}}) t}, \end{aligned}$$

which immediately leads to

$$\psi_2(t) \sim \psi_1(t)^* \psi_1(0) \phi(t), \tag{24}$$

$$\omega_{\mathrm{Lya}} \sim \omega_{acf}/2. \tag{25}$$

The time-oscillating periods T_{acf} and T_{Lya} of the momentum autocorrelation function and the Lyapunov mode are given by $T_{acf} \sim 2\pi/(\tau\omega_{acf})$ and $T_{\mathrm{Lya}} \sim 2\pi/(\tau\omega_{\mathrm{Lya}})$. Using this point and Eq. (25), we obtain our Eq. (20). Note that the above explanation for $T_{\mathrm{Lya}} = 2T_{acf}$ is independent of the number of particles N and the boundary conditions.

In the above explanation, the assumption (23) is crucial, so it may be useful to demonstrate this behavior numerically. Figure 16 shows the autocorrelation function $C_{\mathrm{Lya},x}^{(2N-3)}$ for the longitudinal Lyapunov vector component $\delta x_j^{(2N-3)}$ normalized by its initial value (about 0.0203) in a quasi-one-dimensional system of 50 particles with (H,P) boundary condition. In the autocorrelation function $C_{\mathrm{Lya},x}^{(2N-3)}$, its mean value is subtracted, and an average over the autocorrelation functions of 11 particles in the middle of the system is taken. Here, the Lyapunov index $n = 2N-3$ of the Lyapunov vector component $\delta x_j^{(n)}$ is chosen so that the corresponding Lyapunov step is the first two-point step associated with a time-oscillating Lyapunov mode. In Fig. 16, the numerical data are fitted to a sinusoidal function multiplied by an exponential function, namely, the function (17), with the fitting parameter values $\mathcal{A} \approx 0.967$, $\beta' \approx 1.03 \times 10^{-5}$, $T_{acf} = \tilde{T}_{acf} \approx 4.12 \times 10^3$, and $\xi \approx 1.54$. This time-oscillating period $\tilde{T}_{acf}$ for the autocorrelation function for the longitudinal Lyapunov vector component coincides almost exactly with the time-oscillating period $T_{acf} \approx 4.07 \times 10^3$ of the corresponding Lyapunov mode. This coincidence of the time-oscillating periods supports our assumption Eq. (23) [46].

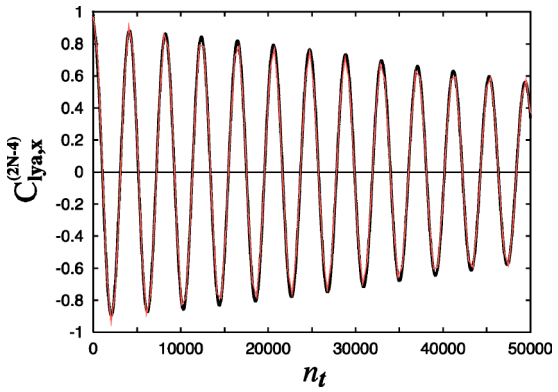

FIG. 16. (Color online) The normalized autocorrelation function $C_{\mathrm{Lya},x}^{(2N-3)}$ for the longitudinal Lyapunov vector component $\delta x_j^{(2N-3)}$ as a function of the collision number n_t for a quasi-one-dimensional system of 50 particles with (H,P) boundary condition. The numerical data are well fitted to a sinusoidal function multiplied by an exponential function.

V. CONCLUSION AND REMARKS

In this paper, we have discussed the relation between the wavelike structure of Lyapunov vectors and the time-oscillating behavior of the momentum autocorrelation functions in quasi-one-dimensional many-hard-disk systems. The quasi-one-dimensional system is a narrow rectangular system in which the x components of the particle positions remained in the same order. This system was proposed as a many-particle system which shows clear stepwise structure of the Lyapunov spectrum (the Lyapunov steps) and wavelike structure of the associated Lyapunov vectors (the Lyapunov modes). Using this system, we showed that there are two types of Lyapunov modes in the spatial and momentum components of the Lyapunov vectors corresponding to the two kinds of steps in the Lyapunov spectrum: one is stationary in time and the other involves a time oscillation. Here, the time-oscillating Lyapunov vectors consist of a simple time-oscillating part plus a momentum proportional time-oscillating part in the longitudinal components, while the transverse time-oscillating Lyapunov vectors consist of a momentum proportional time-oscillating part only. We revealed the phase relation for these time-oscillating Lyapunov modes. It was shown that the system length divided by the time-oscillating period (in real time) of the Lyapunov modes

is independent of the number of particles at the same density, and is of the order of the x component of the thermal velocity. After discussing these wavelike structures of the Lyapunov vectors, we connected them to the time oscillation of the momentum autocorrelation. The time oscillation of the autocorrelation function appears in the longitudinal component of the momentum, and its envelope decays exponentially in time. The main point is that the largest time-oscillating period of the first time-oscillating Lyapunov modes is twice as long as the time-oscillating period of the momentum autocorrelation function. We showed that this relation is independent of the number of particles and the boundary conditions (constructed from combinations of periodic and hard-wall boundary conditions). A simple explanation is given for this relation. It was also shown that the autocorrelation function for the transverse component of the momentum is nicely fitted to the κ-exponential function, implying that it decays exponentially at the beginning and decays as a power after that.

In this paper, we considered mainly a specific boundary condition for the quasi-one-dimensional system: (H,P) hard-wall boundary conditions in the longitudinal direction and periodic boundary conditions in the transverse direction. The system with this boundary condition exhibits a much clear wavelike structure of Lyapunov modes than the purely periodic boundary conditions (P,P), which is a big advantage for quantitative discussions of the Lyapunov modes. Using the (H,P) boundary condition, the spatial translational invariance in the longitudinal direction is violated, and it leads to a different Lyapunov step structure and autocorrelation functions, compared with the (P,P) boundary conditions. For example, in (H,P) the step widths of the Lyapunov spectrum are half of the ones in (P,P), and individual particles can have different momentum autocorrelation functions due to the backscattering effect of the hard wall (see Sec. IV C) while the momentum autocorrelation function is particle-independent for the (P,P) boundary condition. However, as discussed in Ref. [18] for the Lyapunov modes and in Sec. IV C for the autocorrelation functions, there is a simple relation connecting the results obtained from different boundary conditions, so we can predict some of the results of the other boundary conditions from the results for (H,P).

The mode structure of Lyapunov vectors discussed in this paper is related to the structure of the Lyapunov vectors associated with zero-Lyapunov exponents. As explained in the Introduction, there are sets of Lyapunov vector components which take a constant value independent of the particle index, and these quantities corresponding to the stepwise structure of the Lyapunov spectrum have wavelike structures. These are connected with the spatial and time translational invariances and the energy and momentum conservation laws. The results obtained here should generalize to two- and three-dimensional systems with the appropriate changes to the allowed k vectors. However, we need to be careful when making a connection between the conservation laws (or the translation invariances) and the Lyapunov modes. For example, in a system with hard-wall boundary conditions, the spatial translational invariance is violated, but even in such systems the mode structure in the Lyapunov vector component $\delta x_j^{(n)}$ (or $\delta y_j^{(n)}$) can be observed. However, a scenario which suggests that translational invariance is only evident when it is observed in the zero-Lyapunov exponent modes will not predict these observed longitudinal modes.

It should be noted that a time dependence of the Lyapunov modes may not always appear as a time-oscillating behavior. Reference [19] claims that the spatial wave of the Lyapunov vector "moves" at a specific speed in the square system consisting of many hard disks. It is interesting to know how these different behaviors, one oscillating in time and another moving with a speed, can appear.

In some papers, an understanding of the Lyapunov modes was attempted based on an analogy with the hydrodynamic modes [19]. Actually, in both cases the conservation laws like the total momentum conservation and the energy conservation play an essential role, and the longitudinal mode shows a time-dependent behavior. However, it is important to know that the deterministic nature of orbits also plays one of the essential roles in the Lyapunov modes and leads to momentum-proportional time-oscillating components of Lyapunov vectors, although such a characteristic does not appear explicitly in the hydrodynamic mode. In this sense, it is still an open question to see how hydrodynamic modes, which have no concept of a phase-space trajectory, can incorporate time translational invariance.

From results of this paper, it is suggested that there is a connection between the existence of the stepwise structure of Lyapunov spectra and the time oscillations of momentum autocorrelation functions. It is well known that the stepwise structure of the Lyapunov spectra appears clearly in rectangular systems rather than in square systems at the same density. Is it possible to get a similar result for the time oscillation of the momentum autocorrelation function? For example, in a square system with a small number of hard disks we cannot observe the stepwise structure of the Lyapunov spectrum, and in this case the time oscillation of the momentum autocorrelation function does not appear. Therefore, the time oscillations of the autocorrelation function may be useful to understand the condition for the existence of the Lyapunov steps and modes. In this sense, for example, it may be interesting to investigate the time-correlation function in systems with soft-core particle interactions in which the observation of the Lyapunov steps is much harder, and less direct than in systems with hard-core interactions.

ACKNOWLEDGMENTS

One of the authors (T.T.) thanks A. Aliano for suggesting the κ-exponential function. We are grateful for the financial support of this work by the Australian Research Council. One of the authors (T.T.) also appreciates the financial support of the Japan Society for the Promotion of Science.

APPENDIX A: MOMENTUM AUTOCORRELATION FUNCTION OF INDIVIDUAL PARTICLE

In this appendix, we discuss the momentum autocorrelation function of individual particles in the quasi-one-dimensional system with (H,P) boundary conditions. Differ-

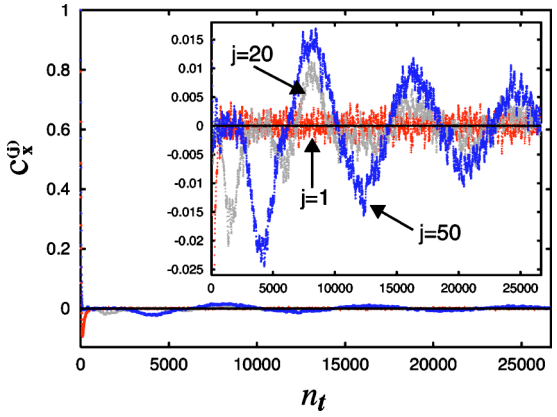

FIG. 17. (Color online) Autocorrelation functions for $c_x^{(1)}$, $c_x^{(20)}$, and $c_x^{(50)}$ for the x components of momenta of the 1st, 20th, and 50th particle, respectively, as functions of the collision number n_t. The system is a quasi-one-dimensional system with $N=100$ and (H,P) boundary condition. The inset: enlarged graphs in the small-magnitude part of the autocorrelation functions.

ent from the (P,P) boundary conditions, the hard-wall boundary in (H,P) violates the translation invariance in the x direction, and this implies that different particles can have different momentum autocorrelation functions.

We introduce the autocorrelation function $c_\eta^{(j)}(t)$ of the jth particle in the η direction at time t ($\eta=x,y$) based on the normalized expression $c_\eta^{(j)}(t)\equiv\tilde{c}_\eta^{(j)}(t)/\tilde{c}_\eta^{(j)}(0)$ with $\tilde{c}_\eta^{(j)}(t)$ defined by

$$\tilde{c}_\eta^{(j)}(t) \equiv \lim_{T\to+\infty} \frac{1}{T}\int_0^T ds p_{kj}(s+t)p_{kj}(s). \qquad \text{(A1)}$$

Using this quantity $\tilde{c}_\eta^{(j)}(t)$, the autocorrelation function $\tilde{C}_\eta(t)$ defined by Eq. (15) is simply given by $\tilde{C}_\eta(t)=[1/(N_2-N_1+1)]\Sigma_{j=N_1}^{N_2}\tilde{c}_\eta^{(j)}(t)$. In this appendix, we show graphs of $c_\eta^{(j)}$ as a function of the collision number $n_t\approx t/\tau$ in the quasi-one-dimensional system of 100 hard disks. We number the particles $1,2,\ldots,N$ from the left to right, as shown in Fig. 1, so, for example, the first and Nth particles are closest to the hard walls.

The first important point about the individual autocorrelation functions is that the time oscillation in the x direction is weak for particles near the walls. This is shown in Fig. 17, where $c_x^{(1)}$ is for the particle nearest to the left hard wall, $c_x^{(50)}$ is the particle most distant from the hard walls, and $c_x^{(20)}$ is a particle between these two extremes. In Fig. 17, the main figure is the full data for these autocorrelation functions, and its inset is an enlarged graph to emphasize the time-oscillating part. This figure shows that we cannot recognize a time-oscillating behavior in $c_x^{(1)}$, the particle nearest to the hard wall, although a clear time oscillation can be recognized in $c_x^{(50)}$, the particle in the middle of the system. We can see a time-oscillating behavior in $c_x^{(20)}$, but its amplitude is smaller than that of $c_x^{(50)}$. The positions of the nodes of the time oscillations of $c_x^{(20)}$ and $c_x^{(50)}$ almost coincide with each other.

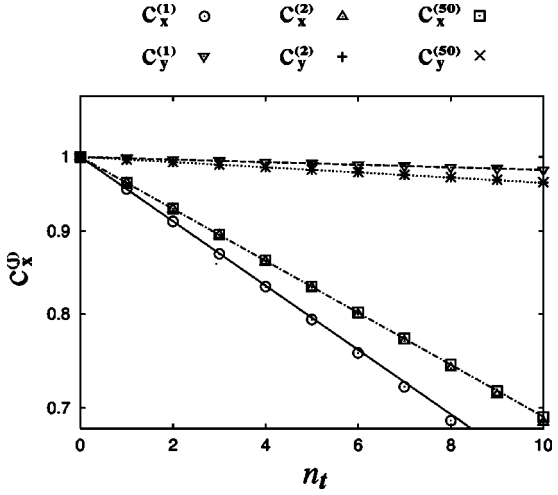

FIG. 18. Exponential decay region of the autocorrelation functions $c_x^{(1)}$ (circles), $c_x^{(2)}$ (triangles), and $c_x^{(50)}$ (squares) as functions of the collision number n_t on a linear-log plot. The solid line (the dotted-broken lines) is a fit of the graph of $c_x^{(1)}$ (the graphs of $c_x^{(2)}$ and $c_x^{(50)}$) to an exponential function. Similar graphs are given for the autocorrelation functions $c_y^{(1)}$ (inverted triangles), $c_y^{(2)}$ (pluses), and $c_y^{(50)}$ (crosses). The broken line (the dotted line) is a fit of the graph of $c_y^{(1)}$ (the graphs of $c_y^{(2)}$ and $c_y^{(50)}$) to an exponential function.

Another difference between individual particle autocorrelation functions appears at short time. Figure 18 shows $c_\eta^{(j)}$, $j=1$, 2, and 50, as functions of the collision number n_t showing the initial damping behavior ($\eta=x,y$). These autocorrelation functions show an exponential decay, which we present as a linear-log plot (straight lines imply exponential decay). This figure shows that the x component (y component) of the autocorrelation function of the particle nearest the hard wall decays faster (slower) than those of other particles, while the damping behavior is always nicely fitted to an exponential function. [In Fig. 18, the graphs are fitted to the exponential function (16) with the fitting parameter values $\alpha'\approx 0.0457$ for $c_x^{(1)}$ (solid line), $\alpha'\approx 0.0369$ for $c_x^{(2)}$ and $c_x^{(50)}$ (dotted-broken line), $\alpha'\approx 0.001\,84$ for $c_y^{(1)}$ (broken line), and $\alpha'\approx 0.003\,68$ for $c_y^{(2)}$ and $c_y^{(50)}$ (dotted line).] This difference may come from the different types of collisions experienced. For the particle nearest the wall, half of the collisions will be with the wall and the other half with the neighboring particle. The x component of the momentum is drastically changed (namely, it changes the sign of p_{xj}), so it may cause a faster decay of the autocorrelation function in the x direction. On the other hand, collisions with the wall effect the y component of the momentum much less, because it is invariant under wall collisions, and does not cause a loss of memory in p_{yj}, leading to a slower decay of the autocorrelation for the first (and Nth) particle in the y direction.

Another point of difference in the autocorrelation functions of individual particles is a negative region which appears after their initial exponential decay. It may be meaningful to mention that a negative region of momentum autocorrelation function has drawn attention previously [47–49]. To discuss such a negative region, in Fig. 19 we show the collision number n_t dependence of the autocorrela-

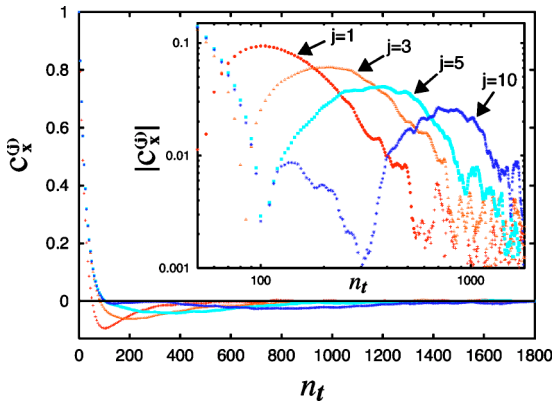

FIG. 19. (Color online) The negative region of autocorrelation functions $c_x^{(1)}$, $c_x^{(3)}$, $c_x^{(5)}$, and $c_x^{(10)}$, as functions of the collision number n_t as a linear-linear plot. The inset: absolute values of the same autocorrelation functions as functions of n_t as a log-log plot.

tion functions $c_x^{(1)}$, $c_x^{(3)}$, $c_x^{(5)}$, and $c_x^{(10)}$. To emphasize the negative region of the autocorrelation function, we show a log-log plot of the absolute values of the same quantities as functions of n_t in the inset to Fig. 20. In this figure, a negative region of the autocorrelation functions appears after the initial exponential decay and before the time oscillations appear. The collision number (or time) at the bottom of this negative region of the autocorrelation function increases, and the amplitude of the bottom decreases, as the particle is farther from the hard-wall (namely, as the particle index j in $c_x^{(j)}$ increases from $j=1$ to 10 in Fig. 20). This phenomenon can be explained by the backscattering effect of the hard walls. Such a backscattering effect is stronger (so the amplitude of the negative region is stronger) in a particle closer to a hard wall. As well the time interval to react to the presence of the wall is longer (so the time at the bottom of the negative region is later) in a particle far from the hard wall. This kind of behavior is not observed in a system in which the boundary conditions in the x direction are periodic.

After the negative region, the time-oscillating part appears. Figure 20 shows the collision number n_t dependence of the autocorrelation functions for $c_x^{(10)}$, $c_x^{(20)}$, $c_x^{(35)}$, and $c_x^{(50)}$ in the collision number region before the time-oscillation

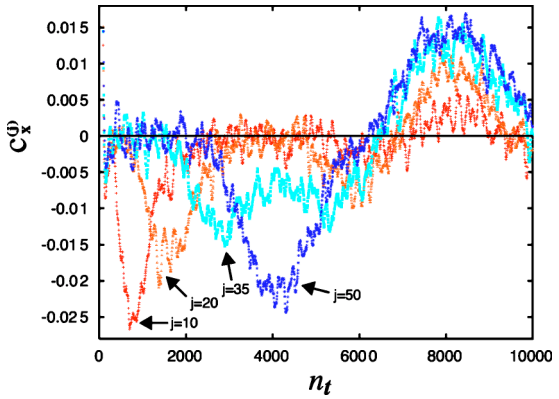

FIG. 20. (Color online) The region before the start of the time oscillation of autocorrelation functions for $c_x^{(10)}$, $c_x^{(20)}$, $c_x^{(35)}$, and $c_x^{(50)}$ as functions of the collision number n_t.

start (about $n_t \approx 6000$ in Fig. 20). The negative peak of the autocorrelation function (discussed in the previous paragraph and indicated by the arrows in Fig. 20) moves to larger collision number n_t as the particle index j increases from $j=10$ to 35 in Fig. 20. On the other hand, the time oscillation of the autocorrelation function starts from about $n_t \approx 6000$, which is independent of the particle index, although the amplitude of the time oscillation is largest for a particle far from the hard walls. Moreover, the time-oscillating period of the autocorrelation function is almost independent of the particle index. These characteristics of the time oscillation of the autocorrelation function suggest that the time-oscillating behavior of the autocorrelation function reflects a collective movement of the system.

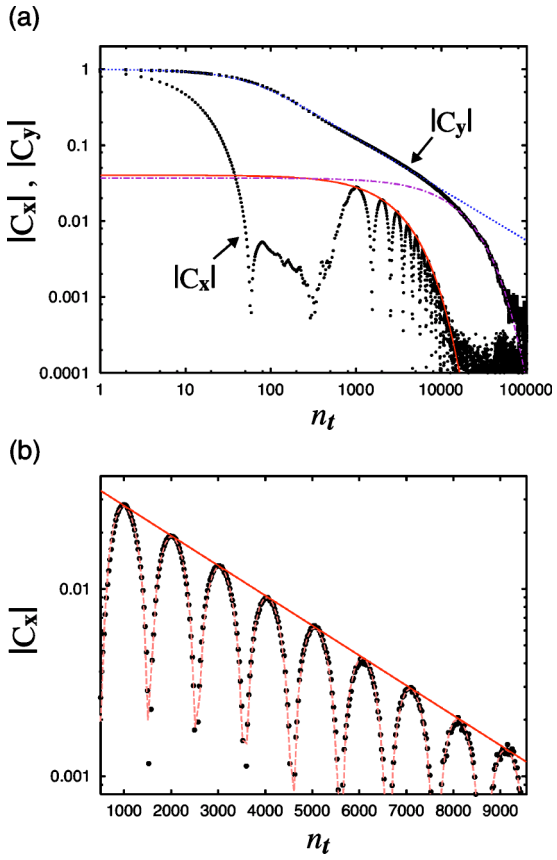

FIG. 21. (Color online) (a) Absolute values $|C_x|$ and $|C_y|$ as functions of the collision number n_t presented as a log-log plot. The solid line is a fit of the envelope of the time-oscillating part of C_x to an exponential function. The dotted line is a fit of C_y to a κ-exponential function [Eq. (18)] and the dotted broken line is a fit to an exponential function in the region where there is a deviation from the κ-exponential function. (b) The time-oscillating part of the autocorrelation part as a graph of the absolute value $|C_x|$ as a function of the collision number n_t presented as a linear-log plot. The broken line is a fit to a sinusoidal function multiplied by an exponential decay function [Eq. (17)], and the solid line is its envelope, which is the same as the solid line in (a). The system is a quasi-one-dimensional system of 50 hard disks with (H,P) boundary conditions.

APPENDIX B: DAMPING BEHAVIOR OF MOMENTUM AUTOCORRELATION FUNCTION IN A LONG TIME INTERVAL

In this appendix, we discuss two points about the momentum autocorrelation function in the long time interval: (i) The shape of the envelope of the time oscillation in C_x, and (ii) The behavior of the autocorrelation function C_y on a much longer time scale than that shown previously.

Figure 21 shows the absolute values of the autocorrelation functions $|C_x|$ and $|C_y|$ as functions of the collision number n_t in a quasi-one-dimensional system of 50 hard disks with (H,P) boundary conditions. In Fig. 21(a), these graphs are plotted as log-log plots, while in Fig. 21(b) the graph for $|C_x|$ is plotted as a linear-log plot. The collision number interval in this figure is about ten times as long as the previous ones, and we took a much longer time average (e.g., over 10^9 collisions).

As shown in Sec. IV A, C_x decays exponentially initially. After the initial decay, the time-oscillating region of C_x starts. We fitted this region of C_x to a sinusoidal function multiplied by an exponential function, namely, Eq. (17), with the fitting parameters $\mathcal{A} \approx 0.0402$, $\beta' \approx 0.000\,368$, $T_{acf} \approx 2.03 \times 10^3$, and $\xi \approx 1.53$ as the broken lines in Fig. 21(b). The solid lines in Figs. 21(a) and 21(b) are the envelope $C_x = \mathcal{A} \exp\{-\beta' n_t\}$ of this function. In order to see its exponential behavior, we show in Fig. 21(b) the linear-log plot of $|C_x|$ for the time-oscillating region of C_x, in which the exponential decay is represented as a straight line. In this linear-log plot, the local maximum points of $|C_x|$ are clearly on a straight line.

In Sec. IV A we also showed that C_y is nicely fitted to a κ-exponential function (18). This is also shown in Fig. 21(a) as the fit line to the κ-exponential function with fitting parameter values $\alpha'' \approx 0.007\,46$ and $\kappa \approx 1.48$ (dotted line). However, Fig. 21(a) shows that there is a deviation from this functional form on a longer time scale. Such a deviation is significant when $n_t > 10\,000$ in this graph. We fitted C_y to an exponential function $C_y = \mathcal{A}' \exp\{-\alpha''' n_t\}$ with fitting parameter values $\mathcal{A}' \approx 0.0369$ and $\alpha''' \approx 6.25 \times 10^{-5}$ [the dotted-broken line in Fig. 21(a)] in the region where C_y deviates from the κ exponential.

[1] P. Gaspard, *Chaos, Scattering and Statistical Mechanics* (Cambridge University Press, Cambridge, 1998).
[2] J. R. Dorfman, *An Introduction to Chaos in Nonequilibrium Statistical Mechanics* (Cambridge University Press, Cambridge, 1999).
[3] U. Dressler, Phys. Rev. A **38**, 2103 (1988).
[4] D. J. Evans, E. G. D. Cohen, and G. P. Morriss, Phys. Rev. A **42**, 5990 (1990).
[5] C. P. Dettmann and G. P. Morriss, Phys. Rev. E **53**, R5545 (1996).
[6] T. Taniguchi and G. P. Morriss, Phys. Rev. E **66**, 066203 (2002).
[7] K. Kaneko, Physica D **23**, 436 (1986).
[8] R. Livi and S. Ruffo, in *Nonlinear Dynamics*, edited by G. Turchetti (World Scientific, Singapore, 1989), p. 220.
[9] M. Falcioni, U. M. B. Marconi, and A. Vulpiani, Phys. Rev. A **44**, 2263 (1991).
[10] Lj. Milanović and H. A. Posch, J. Mol. Liq. **96–97**, 221 (2002).
[11] T. Taniguchi and G. P. Morriss, Phys. Rev. E **68**, 046203 (2003).
[12] G. Paladin and A. Vulpiani, J. Phys. A **19**, 1881 (1986).
[13] C. M. Newman, Commun. Math. Phys. **103**, 121 (1986).
[14] Ya. G. Sinai, Int. J. Bifurcation Chaos Appl. Sci. Eng. **6**, 1137 (1996).
[15] T. Taniguchi, C. P. Dettmann, and G. P. Morriss, J. Stat. Phys. **109**, 747 (2002).
[16] Ch. Dellago, H. A. Posch, and W. G. Hoover, Phys. Rev. E **53**, 1485 (1996).
[17] H. A. Posch and R. Hirschl, in *Hard Ball Systems and the Lorentz Gas*, edited by D. Szász (Springer-Verlag, Berlin, 2000), p. 279.
[18] T. Taniguchi and G. P. Morriss, Phys. Rev. E **68**, 026218 (2003).
[19] C. Forster, R. Hirschl, H. A. Posch, and W. G. Hoover, Physica D **187**, 294 (2004).
[20] J.-P. Eckmann, C. Forster, H. A. Posch, and E. Zabey, e-print nlin.CD/0404007.
[21] H. Yang and G. Radons, e-print nlin.CD/0404027.
[22] C. Forster and H. A. Posch, e-print nlin.CD/0409019.
[23] J.-P. Eckmann and O. Gat, J. Stat. Phys. **98**, 775 (2000).
[24] T. Taniguchi and G. P. Morriss, Phys. Rev. E **65**, 056202 (2002).
[25] S. McNamara and M. Mareschal, Phys. Rev. E **64**, 051103 (2001).
[26] M. Mareschal and S. McNamara, Physica D **187**, 311 (2004).
[27] A. S. de Wijn and H. van Beijeren, Phys. Rev. E **70**, 016207 (2004).
[28] R. Zwanzig, Phys. Rev. **156**, 156 (1967).
[29] A. Rahman, Phys. Rev. Lett. **19**, 420 (1967).
[30] D. Levesque, L. Verlet, and J. Kürkijarvi, Phys. Rev. A **7**, 1690 (1973).
[31] M. Berkowitz and J. A. McCammon, J. Chem. Phys. **75**, 957 (1981).
[32] W. E. Alley, B. J. Alder, and S. Yip, Phys. Rev. A **27**, 3174 (1983).
[33] J. P. Hansen and I. R. McDonald, *Theory of Simple Liquids*, 2nd ed. (Academic Press, London, 1990).
[34] J. R. D. Copley and S. W. Lovesey, Rep. Prog. Phys. **38**, 461 (1975).
[35] A. A. van Well, P. Verkerk, L. A. de Graaf, J.-B. Suck, and J. R. D. Copley, Phys. Rev. A **31**, 3391 (1985).
[36] W. Schaertl and C. Roos, Phys. Rev. E **60**, 2020 (1999).
[37] R. Kubo, M. Toda, and N. Hashitsume, *Statistical Physics II, Nonequilibrium Statistical Mechanics* (Springer-Verlag, Berlin, 1985).
[38] I. M. de Schepper, E. G. D. Cohen, C. Bruin, J. C. van Rijs, W. Montfrooij, and L. A. de Graaf, Phys. Rev. A **38**, 271 (1988).

[39] R. Zwanzig, Phys. Rev. **124**, 983 (1961).
[40] G. Benettin, L. Galgani, and J.-M. Strelcyn, Phys. Rev. A **14**, 2338 (1976).
[41] I. Shimada and T. Nagashima, Prog. Theor. Phys. **61**, 1605 (1979).
[42] G. Benettin, L. Galgani, A. Giorgilli, and J.-M. Strelcyn, Meccanica **15**, 9 (1980).
[43] G. Benettin, L. Galgani, A. Giorgilli, and J.-M. Strelcyn, Meccanica **15**, 21 (1980).
[44] V. I. Arnold, *Mathematical Methods of Classical Mechanics*, 2nd ed. (Springer-Verlag, New York, 1989).
[45] G. Kaniadakis, Physica A **296**, 405 (2001).
[46] It should be noted that the autocorrelation function $C_{\mathrm{Lya},x}^{(2N-3)}$ includes an effect due to the longitudinal Lyapunov mode without momentum [the x component of the second term on the right-hand side of Eq. (2)] as well as the momentum proportional term [the x component of the first term on the right-hand side of Eq. (2)]. On the other hand, the assumption (23) is for the term for the momentum proportional Lyapunov mode only. In this sense, Fig. 16 does not exactly represent a proof of the assumption (23).
[47] A. Rahman, Phys. Rev. **136**, A405 (1964).
[48] B. J. Berne, J. P. Boon, and S. A. Rice, J. Chem. Phys. **45**, 1086 (1966).
[49] R. Zwanzig and M. Bixon, Phys. Rev. A **2**, 2005 (1970).